Human information processing in complex networks

Christopher W. Lynn[1], Lia Papadopoulos[1], Ari E. Kahn[2,3], & Danielle S. Bassett[1,3,4,5,6,*]

[1]*Department of Physics & Astronomy, College of Arts & Sciences, University of Pennsylvania, Philadelphia, PA 19104, USA*

[2]*Department of Neuroscience, Perelman School of Medicine, University of Pennsylvania, Philadelphia, PA 19104, USA*

[3]*Department of Bioengineering, School of Engineering & Applied Science, University of Pennsylvania, Philadelphia, PA 19104, USA*

[4]*Department of Electrical & Systems Engineering, School of Engineering & Applied Science, University of Pennsylvania, Philadelphia, PA 19104, USA*

[5]*Department of Neurology, Perelman School of Medicine, University of Pennsylvania, Philadelphia, PA 19104, USA*

[6]*Department of Psychiatry, Perelman School of Medicine, University of Pennsylvania, Philadelphia, PA 19104, USA*

Humans communicate using systems of interconnected stimuli or concepts – from language and music to literature and science – yet it remains unclear how, if at all, the structure of these networks supports the communication of information. Although information theory provides tools to quantify the information produced by a system,[1–7] traditional metrics do not account for the inefficient and biased ways that humans process this information.[8–11] Here we develop an analytical framework to study the information generated by a system as perceived by a human observer. We demonstrate experimentally that this perceived information depends critically on a system's network topology. Applying our framework to several real networks, we find that they communicate a large amount of information (having high entropy) and do so efficiently (maintaining low divergence from human expectations). Moreover, we show that such efficient communication arises in networks that are simultaneously heterogeneous, with high-degree hubs, and clustered, with tightly-connected modules – the two defining features of hierarchical organization. Together, these results suggest that many real networks are constrained by the pressures of information transmission, and that these pressures select for specific structural features.

Humans receive information in discrete chunks, which transition from one to another – as words in a sentence or notes in a musical progression – to create coherent messages. The networks formed by these chunks (nodes) and transitions (edges) encode the structure of allowed messages, fundamentally constraining the ways that we communicate with one another. Although attempts to study the information properties of such transition networks date to the foundation of information theory itself,[1] with applications to linguistics,[6,8] music theory,[7] social and information networks,[2,3] the Internet,[4] and transportation,[5] fundamental questions concerning the impact of network structure on how humans process information remain unanswered. The primary difficulty is accounting for the human perspective: formally, a message's information content is not inherent, but rather depends crucially on the expectations (or prior probabilities) of a receiver.[1,8,12] Whereas for computers prior probabilities are often prescribed, human expectations are biased[9] and differ from person to person,[8] with important consequences for behavior[10] and cognition.[11] Recently, advances in psychology and neuroscience have shed light on how humans learn and internally estimate the structure of complex probabilistic systems.[13–17] Given this progress, it is now possible and compelling to build a framework to quantify human information processing and to consider what types of networks support efficient communication.

We set out to study the amount of information a human perceives when observing a sequence of stimuli. Naturally, one might expect a human to perceive roughly the same amount of information as is being produced by a sequence, or its entropy.[1,12] Here, to motivate our analytic results, we carry out a set of experiments showing that these two quantities – perceived information and produced information (entropy) – differ systematically. To measure perceived information, we employ a paradigm recently developed in statistical learning,[15–17] presenting subjects with sequences of stimuli on a screen (Fig. 1a) and asking them to respond to each stimulus by pressing the indicated keys on a keyboard (Fig. 1b). Although many real communication systems have long-range correlations, the production of information is traditionally modeled using a Markov process,[1,12] or equivalently, a random walk on a (possibly weighted, directed) network.[2] Therefore, we assign each stimulus to a node in an underlying network, and we stipulate the order of sequences using random walks (Fig. 1a; Methods). By measuring subjects' reaction times, we can infer how much

information they perceive: slow reactions reflect surprising transitions (with high perceived information) , while fast reactions indicate expected transitions (with low perceived information).[10,16,17]

The amount of information produced by a transition from one stimulus i to another j is $\log k_i$, where k_i is the degree of node i.[12] Indeed, subjects' reaction times are remarkably well-predicted by this quantity, with each additional bit of information inducing a linear 32 ms increase in reaction times (Fig. 1c). However, even if we present subjects with networks of constant degree – forcing each transition to produce identical information – we still discover consistent variations in reaction times driven by network topology. For example, consider the modular network in Fig. 1d, which by symmetry only contains three types of transitions. Each transition produces reaction times that are distinct from the other two (Fig. 1e), with transitions between or at the boundaries of modules generating more surprise than those deep within a module. Moreover, when compared against random networks of constant degree, reactions in the modular graph are significantly faster overall (Fig. 1f), indicating a decrease in perceived information. Together, these results reveal that humans perceive information, beyond the information produced by a sequence, in a manner that depends systematically on network topology.

The differences between perceived information and produced information (entropy) stem from the inaccuracy of human expectations. While a transition $i \to j$ produces $-\log P_{ij}$ bits of information, where P is the transition probability matrix, a person with expectations based on an estimated transition matrix $\hat{P}$ will perceive $-\log \hat{P}_{ij}$ bits of information. Although several models have been proposed for how humans estimate probabilistic systems,[14,15] converging evidence indicates that humans integrate sequential signals over time,[17–19] yielding expectations that include higher powers of the transition matrix: $\hat{P} = C\sum_{t=0}^{\infty} g(t)P^{t+1}$, where $g(t) \geq 0$ is a decreasing function and $C = (\sum_t g(t))^{-1}$ is a normalization constant. We study a number of choices for $g(t)$ in Supplemental Sec. 6.2, but here we focus on the specific example $g(t) = \eta^t$, where $\eta \in (0, 1)$ represents the inaccuracy of a person's expectations. We note that this model can be derived from temporal context learning in psychology,[19] appears in reinforcement learning,[18,19] and emerges from the free energy principle in physics.[17] Inferring η from each subject's reaction times (Meth-

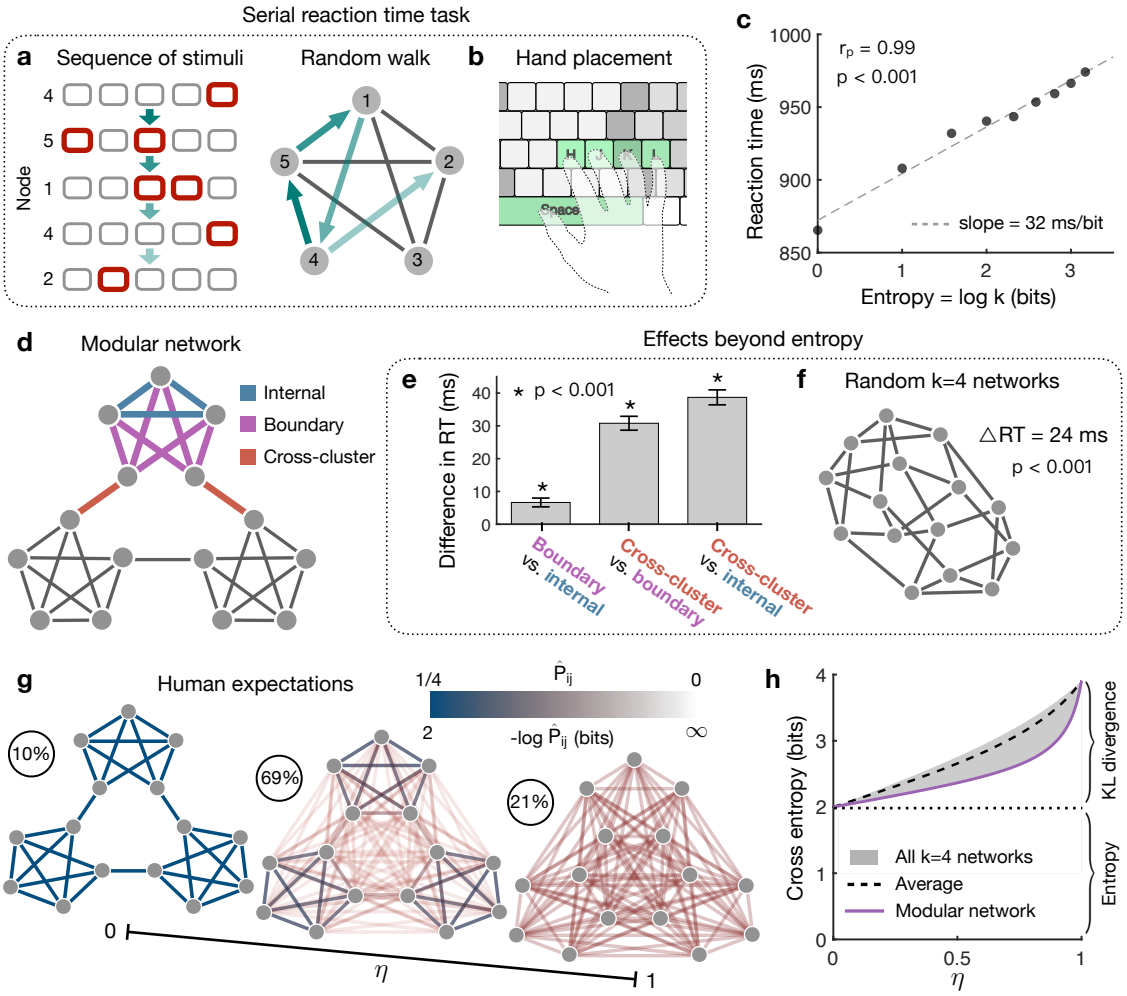

Fig. 1 | Human behavioral experiments reveal the dependence of perceived information on network topology.

a, **b**, Experimental setup for serial reaction time tasks. Subjects are shown sequences of 1500 stimuli, each consisting of five squares with one or two highlighted in red, the order of which is determined by a random walk on an underlying network (**a**). Subjects press keys on a keyboard corresponding to the highlighted squares (**b**). **c**, Reaction times, averaged over all transitions following nodes of a given degree k, compared with the entropy of the transition $\log k$ (Pearson correlation coefficient $r_p = 0.99$, $p < 0.001$). A random network of $N = 15$ nodes and $E = 30$ edges is generated for each subject (177 subjects). Additionally, to account for inter-subject variability, we estimate a mixed effects model, finding an effect size of 26 ms/bit ($p < 0.001$; Supplementary Sec. 5.1). **d**, Modular network with three modules of five nodes each. **e**, **f**, Effects of network topology on reaction times after controlling for entropy. Effect sizes and p-values are estimated using mixed effects models (Supplementary Sec. 5.2

and 5.3). In the modular network, each type of transition produces reaction times distinct from the other two (**e**; 173 subjects). Compared with random networks of equal entropy – that is, random networks of constant degree 4 – the modular network induces consistently faster reactions (**f**; 84 subjects). **g**, Internal estimate $\hat{P}$ of the transition probabilities in the modular network for $\eta \to 0$ (left), $\eta \to 1$ (right), and intermediate η (middle). Percentages indicate proportion of subjects, across all tasks, whose behavior corresponds to each category (Supplementary Sec. 4). **h**, Cross entropy $S(P, \hat{P})$ as a function of η for all k-4 networks of $N = 15$ nodes (shaded region), the average over all k-4 networks (dashed line), and the modular network (solid line).

ods), we find that 10% of subjects hold exact estimates of the transition structure ($\eta \to 0$), while 21% have expectations that are completely disordered ($\eta \to 1$; Fig. 1g). Importantly, most people's expectations are only partially disordered (Fig. S1), which yields an increase in perceived information for between- versus within-module transitions in the modular network (Figs. 1g and S2). In turn, this difference in perceived information explains the effects on reaction times observed in the modular network (Fig. 1e).

We are now prepared to study the perceived information of an entire communication system. Averaging over the random walk process, we have $\langle -\log \hat{P}_{ij} \rangle_P = -\sum_{ij} \pi_i P_{ij} \log \hat{P}_{ij}$, where $\boldsymbol{\pi}$ is the stationary distribution of P. Interestingly, this quantity – known as the cross entropy $S(P, \hat{P})$ between P and $\hat{P}$ – splits naturally into the entropy $S(P)$, or the amount of produced information, and the KL divergence $D_{\text{KL}}(P||\hat{P})$, or the inefficiency of the observer's expectations:

$$\underbrace{\langle -\log \hat{P}_{ij} \rangle_P}_{S(P,\hat{P})} = \underbrace{\langle -\log P_{ij} \rangle_P}_{S(P)} + \underbrace{\langle -\log \frac{\hat{P}_{ij}}{P_{ij}} \rangle_P}_{D_{\text{KL}}(P||\hat{P})}. \tag{1}$$

This relationship has a number of immediate consequences, including the fact that perceived information $S(P, \hat{P})$ is lower bounded by produced information $S(P)$ (since $D_{\text{KL}}(P||\hat{P}) \geq 0$) and that inefficiency is minimized when a person's expectations are exact (since $D_{\text{KL}}(P||\hat{P}) = 0$ only when $\hat{P} = P$).[12] For example, consider the set of degree-4 networks from our human experiments (Fig. 1f). While all such networks have identical entropy, their differing topologies induce a range of

cross entropies (Fig. 1h). Notably, the modular graph displays relatively low cross entropy across all values of η, thus matching the observed decrease in subjects' reaction times (Fig. 1f).

Using the framework developed above, we are ultimately interested in characterizing the perceived information generated by real communication systems. The networks chosen (Table 1) have all either evolved or been designed to communicate information through sequences of stimuli (such as words or notes) or concepts (such as scientific papers, websites, or social interactions). Strikingly, we find that the networks share two consistent properties: they produce large amounts of information (high entropy; Fig. 2a) while at the same time maintaining low inefficiency (low KL divergence; Fig. 2b). Specifically, these properties hold relative to completely randomized versions of the networks (Table 1). Interestingly, different network types exhibit these information properties to varying degrees (Fig. 2c). For example, language networks have the highest entropy but also the highest KL divergence, perhaps reflecting the pressure on language to maximize information rate. Meanwhile, music networks are low in both entropy and KL divergence, mirroring their role as a means for entertainment rather than rapid communication. If we instead compare the real networks against randomized versions that preserve node degrees,[20] we find that the entropy is unchanged (Fig. 2d), indicating that produced information depends only on the degree distribution. By contrast, even compared to these entropy-preserving networks, the KL divergence of real networks remains low (Fig. 2e). We verify that these results hold for (i) various values of η, (ii) different models for $\hat{P}$, and (iii) directed versions of the above networks (Supplementary Sec. 6).

Given the high entropy and low KL divergence displayed by real networks, it is natural to wonder what structural features give rise to these properties. To begin, for undirected networks one can show that $S = \sum_i k_i \log k_i$, confirming that the entropy of a network is determined by its degree sequence (Fig. 2d). It is clear that the entropy grows with increasing node degrees, supporting the intuition that denser networks yield more complex random walks. Moreover, since S is convex in $\boldsymbol{k}$, the entropy is larger for networks with a small number of high-degree nodes and many low-degree nodes. Interestingly, such heterogeneous structure is characteristic of scale-free networks[21] and has been observed in human language,[22] the Internet,[21] and social networks.[23] To

Table 1 | Properties of the real communication networks examined in this paper

Type / Name	N	E	S^{real} (bits)	S^{rand} (bits)	$D_{\text{KL}}^{\text{real}}$ (bits)	$D_{\text{KL}}^{\text{rand}}$ (bits)
Language (word transitions)						
Shakespeare	11,234	97,892	6.15	4.16	1.74	2.17
Homer	3,556	23,608	5.25	3.79	1.75	2.12
Plato	2,271	9,796	4.41	3.19	1.74	2.04
Jane Austen	1,994	12,120	4.92	3.66	1.71	2.10
William Blake	370	781	2.59	2.24	1.64	1.77
Miguel de Cervantes	6,090	43,682	5.55	3.89	1.76	2.14
Walt Whitman	4,791	16,526	4.24	2.89	1.76	2.00
Semantic relationships						
Bible	1,707	9,059	4.31	3.48	1.45	2.07
Les Miserables	77	254	3.25	2.82	0.84	1.65
Edinburgh Thesaurus	7,754	226,518	6.26	5.88	2.07	2.21
Roget Thesaurus	904	3,447	3.19	3.02	1.76	1.99
Glossary terms	60	114	2.32	2.09	1.29	1.55
FOLDOC	13,274	90,736	4.11	3.83	1.72	2.14
ODLIS	1,802	12,378	4.59	3.83	1.70	2.11
World Wide Web						
Google internal	12,354	142,296	6.15	4.56	1.35	2.19
Education	2,622	6,065	3.01	2.36	0.92	1.85
EPA	2,232	6,876	3.34	2.74	1.75	1.95
Indochina	9,638	45,886	3.88	3.33	0.58	2.08
2004 Election blogs	793	13,484	5.78	5.11	1.36	2.01
Spam	3,796	36,404	5.30	4.30	1.66	2.16
WebBase	6,843	16,374	3.48	2.41	1.09	1.87
Citations						
arXiv Hep-Ph	12,711	139,500	5.02	4.49	1.68	2.19
arXiv Hep-Th	7,464	115,932	5.56	4.98	1.64	2.20
Cora	3,991	16,621	3.50	3.14	1.48	2.04
DBLP	240	858	3.30	2.93	1.37	1.88
Social relationships						
Facebook	13,130	75,562	4.22	3.59	1.78	2.11
arXiv Astr-Ph	17,903	196,972	5.39	4.49	1.41	2.19
Adolescent health	2,155	8,970	3.22	3.14	1.78	2.03
Highschool	67	267	3.11	3.07	1.15	1.57
Jazz	198	2,742	5.09	4.81	0.94	1.61
Karate club	34	78	2.58	2.32	1.05	1.40
Music (note transitions)						
Thriller – Michael Jackson	67	446	4.03	3.78	0.76	1.38
Hard Day's Night – Beatles	41	212	3.62	3.42	0.49	1.21
Bohemian Rhapsody – Queen	71	961	5.01	4.77	0.55	0.95
Africa – Toto	39	163	3.41	3.13	0.84	1.29
Sonata No 11 – Mozart	55	354	3.91	3.73	0.83	1.28
Sonata No 23 – Beethoven	69	900	4.86	4.72	0.65	0.96
Nocturne Op 9-2 – Chopin	59	303	3.62	3.42	0.95	1.43
Clavier Fugue 13 – Bach	40	143	3.06	2.92	0.89	1.37
Ballade Op 10-1 – Brahms	69	670	4.42	4.31	0.80	1.18

For each network we list its type and name, number of nodes N and edges E, entropy of the real network S^{real} and after randomizing the edges S^{rand}, and KL divergence of the real network $D_{\text{KL}}^{\text{real}}$ and after randomization $D_{\text{KL}}^{\text{rand}}$ with η set to the average value 0.80 from our experiments. S^{rand} and $D_{\text{KL}}^{\text{rand}}$ are averaged over 100 randomizations. For descriptions and references see Supplementary Sec. 10.

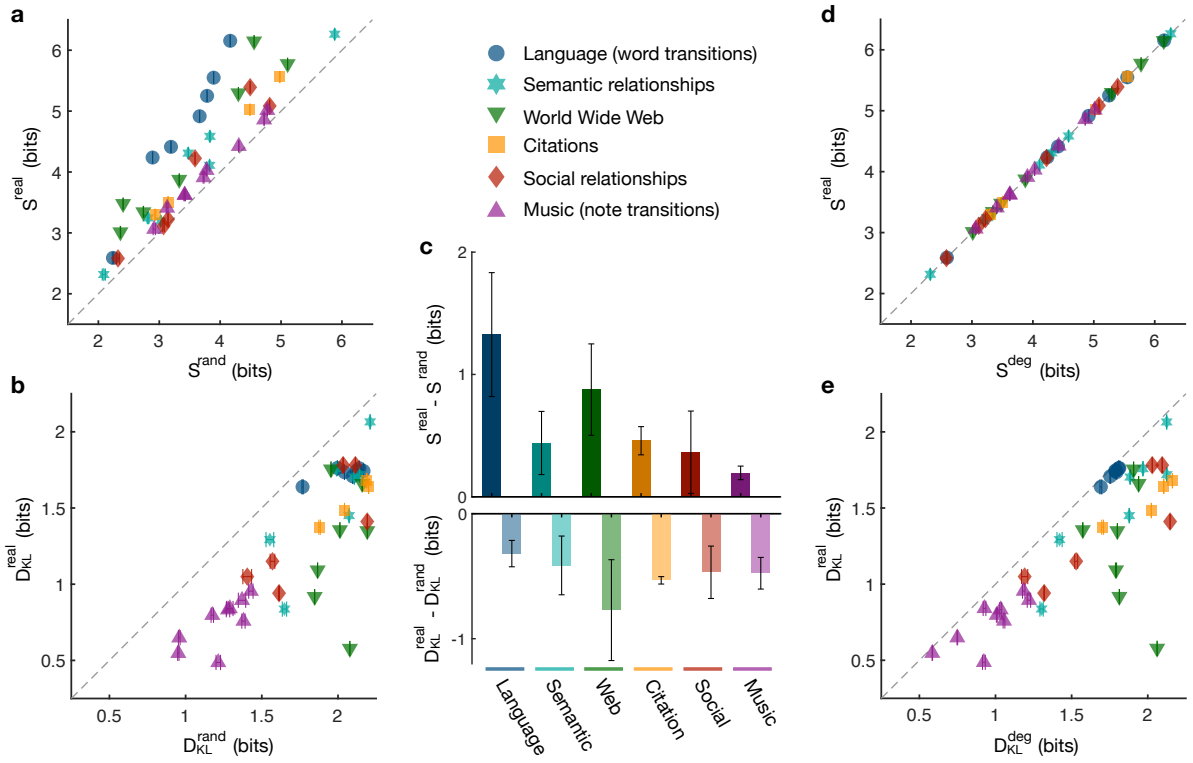

Fig. 2 | The entropy and KL divergence of real networks.

a, Entropy of fully randomized versions of the networks listed in Table 1 (S^{rand}) compared with the true value (S^{real}). **b**, KL divergence of fully randomized versions of the real networks ($D_{\text{KL}}^{\text{rand}}$) compared with the true value ($D_{\text{KL}}^{\text{real}}$), with η set to the average value 0.80 from our experiments (Supplementary Sec. 4). **c**, Difference between S^{real} and S^{rand} (top) and difference between $D_{\text{KL}}^{\text{real}}$ and $D_{\text{KL}}^{\text{rand}}$ (bottom) for different network types, with error bars indicating standard deviation over networks of each type. **d**, Entropy of degree-preserving randomized networks (S^{deg}) compared with S^{real}. **e**, KL divergence of degree-preserving randomized networks ($D_{\text{KL}}^{\text{deg}}$) compared with $D_{\text{KL}}^{\text{real}}$ with fixed $\eta = 0.80$. In panels **a**, **b**, **d**, and **e**, data points and error bars (standard deviations) are estimated from 100 realizations of the randomized networks. All networks are undirected; for examination of directed versions see Supplementary Sec. 6.

investigate the relationship between a network's entropy and its degree distribution, we can derive a number of analytic results in the thermodynamic limit $N \to \infty$ (Supplementary Sec. 7). For example, the entropy of an Erdös-Rényi network is given by $S \approx \log\langle k\rangle$ for large average degree $\langle k\rangle$. For scale-free networks with degree exponent γ (Fig. 3a), we find that $S = \log\langle k\rangle + \frac{1}{\gamma-2} - \log\frac{\gamma-1}{\gamma-2}$, indicating that $\gamma = 2$ is a critical exponent since the entropy diverges as $\gamma \to 2$. Generating ensem-

bles of Erdös-Rényi and scale-free networks, we numerically verify the logarithmic dependence of S on $\langle k \rangle$ (Fig. 3b). Moreover, we find that S increases for decreasing γ (Fig. 3c), suggesting that the entropy grows with increasing degree heterogeneity, which we also confirm numerically (Fig. 3d). This final result reveals that, after controlling for edge density, the entropy is largest for networks with heavy-tailed degree distributions.

In contrast to the entropy, the KL divergence depends on the expectations of an observer. As these expectations become more accurate (that is, as η decreases), we expect $D_{\mathrm{KL}}(P||\hat{P})$ to decrease (Fig. 1h). For an undirected network with adjacency matrix G, we can expand in the limit of small η to find that $D_{\mathrm{KL}} \approx -\log(1-\eta) - \frac{\eta}{2E\ln 2}\sum_i \frac{1}{k_i}\triangle_i$, where $\triangle_i = (G^3)_{ii}$ is the number of (possibly weighted) triangles involving node i (Supplementary Sec. 8). In addition to decreasing with η, we see that D_{KL} is smaller for networks with a large number of triangles, explaining, for example, the low KL divergence of the modular network (Fig. 1h). Indeed, an abundance of triangles is typically associated with modular structure, a ubiquitous feature of real communication networks, from social and scientific interactions[2,26] to language[27] and the Internet.[28] To investigate the impact of modularity on the KL divergence, we can derive analytic expressions for D_{KL} that hold for all values of η in the thermodynamic limit (Supplementary Sec. 8). For example, the KL divergence of an Erdös-Rényi network is given by $D_{\mathrm{KL}} = -\log(1-\eta)$. For block networks with communities of size n and a fraction of within-community edges f (Fig. 3e), we find that $D_{\mathrm{KL}} = -\log\left[1-\eta\left(1-\frac{\langle k\rangle}{n}\frac{(1-\eta)f^3}{1-\eta f}\right)\right]$. Generating sets of Erdös-Rényi and block networks, we confirm the analytic predictions that D_{KL} grows with increasing η (Fig. 3f) and decreases for increasing modularity (Fig. 1g) and clustering (Fig. 1h). Therefore, even after controlling for the inaccuracy η of human expectations, we find that modular organization helps to decrease communication inefficiency.

To attain both the high entropy and low KL divergence observed in real systems, it appears that networks must be simultaneously heterogeneous and modular, the two defining features of hierarchical organization.[29] In order to test this hypothesis, we develop a model that combines the heterogeneous degrees of scale-free networks with the modular structure of block networks (Fig.

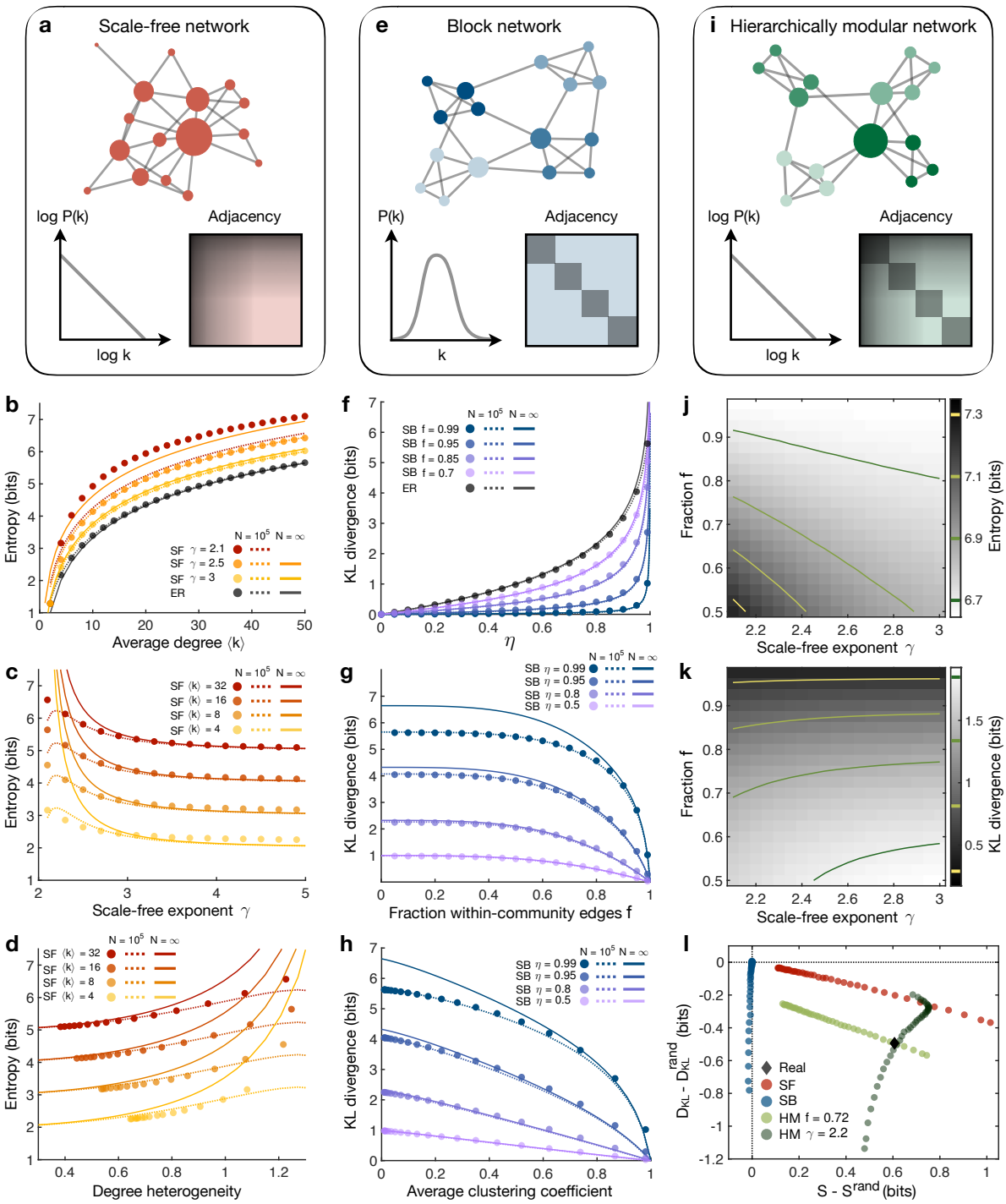

Fig. 3 | The impact of network topology on entropy and KL divergence.

a, Scale-free (SF) network, characterized by a power-law degree distribution and the presence of high-degree hub nodes. **b**, Entropy as a function of $\langle k \rangle$ for Erdös-Rényi (ER) and SF networks with different values of γ. Data points are exact calculations for ER and SF

networks generated using the static model[24] with $N = 10^4$. Lines are derived from the expected degree distributions: dashed lines are numerical results for $N = 10^4$ and solid lines are analytic results for $N \to \infty$ (Supplementary Sec. 7). Note that the thermodynamic limit for $\gamma = 2.1$ does not appear in the displayed range. **c**, Entropy as a function of γ for SF networks with fixed $\langle k \rangle$. In the thermodynamic limit (solid lines), the entropy diverges as $\gamma \to 2$, while the analytic results are nearly exact for $\gamma > 3$. **d**, Entropy as a function of degree heterogeneity $H = \langle |k_i - k_j| \rangle / \langle k \rangle$, where $\langle |k_i - k_j| \rangle$ is the absolute difference in degrees averaged over all pairs of nodes,[25] for SF networks with fixed $\langle k \rangle$ and variable γ. **e**, Stochastic block (SB) network, characterized by dense connectivity within communities and sparse connectivity between communities. **f**, KL divergence as a function of η for ER and SB networks with communities of size $n = 100$ and different values of f. Data points are exact calculations for networks with $N = 10^4$ and $\langle k \rangle = 100$, and lines are analytic calculations for $N = 10^4$ (dashed) and $N \to \infty$ (solid; Supplementary Sec. 8). **g**, KL divergence as a function of f for SB networks with fixed η. The analytic results are nearly exact for $\eta < 0.8$. **h**, KL divergence as a function of the average clustering coefficient for SB networks with fixed η and variable f. **i**, Hierarchically modular (HM) network, characterized by a power-law degree distribution and modular structure (Supplementary Sec. 9). **j**, Entropy as a function of γ and f for HM networks with $N = 10^4$, $\langle k \rangle = 100$, and $n = 100$. **k**, KL divergence as a function of γ and f for HM networks with η set to the average value 0.80 from our experiments. **l**, Average entropies and KL divergences of real and model networks compared to fully randomized versions. Data points are averages over the set of networks in Table 1, where for each real network we generate SF networks with variable γ (red), SB networks with communities of size $n \approx \sqrt{N}$ and variable f (blue), and HM networks with $n \approx \sqrt{N}$ and variable γ (fixed $f = 0.72$; light green) or variable f (fixed $\gamma = 2.2$; dark green), all with N and E equal to the real network. HM networks with $\gamma = 2.2$ and $f = 0.72$ match the average entropy and KL divergence of real networks.

3i; Supplementary Sec. 9). By adjusting γ and f, we show that these hierarchically modular networks display both a range of entropies (Fig. 3j) and KL divergences (Fig. 3k). In fact, while scale-free networks do not exhibit the low KL divergence of real networks nor do block networks display their high entropy, we find that hierarchically modular networks can attain both properties (Fig. 3l). Taken together, these results indicate that heterogeneity and modularity, precisely the features commonly observed in real communication systems,[2,21–23,26–29] are both required to

achieve high information production and low inefficiency.

In this study, we develop tools to quantify human information processing in complex networks. We find that real networks support the rapid and efficient transmission of information, and that this efficient communication emerges as a consequence of hierarchical organization. These results raise a number of questions concerning the relationship between human cognition and the structure of communication systems. For example, how has language evolved over time – or perhaps even co-evolved with the brain[30] – to facilitate information transmission? Furthermore, how can we design communication systems, from technology[31] to classroom lectures,[32] to optimize efficient communication? The framework presented here provides the mathematical tools to begin answering these questions.

Methods

Experimental setup. Subjects performed a self-paced serial reaction time task using a computer screen and keyboard. Each stimulus was presented as a horizontal row of five grey squares; all five squares were shown at all times. The squares corresponded spatially with the keys 'Space', 'H', 'J', 'K', and 'L' (Fig. 1b). To indicate a target key or pair of keys for the subject to press, the corresponding squares would become outlined in red (Fig. 1a). When subjects pressed the correct key combination, the squares on the screen would immediately display the next stimulus. If an incorrect key or pair of keys was pressed, the message 'Error!' was displayed on the screen below the stimulus and remained until the subject pressed the correct key(s). The order in which stimuli were presented to each subject was determined by a random walk on a network of $N = 15$ nodes. For each subject, one of the 15 key combinations was randomly assigned to each node in the network (Fig. 1a).

In the first experiment, each subject was assigned a random Erdös-Rényi network with $E = 30$ edges. In the second experiment, all subjects responded to sequences of stimuli drawn from the modular network (Fig. 1d). We remark that each node in the modular network is connected to four other nodes, so the entropy of each transition was a constant $-\log \frac{1}{4} = 2$ bits. Some subjects performed both of the first two experiments in back to back stages, with the order of the experiments counterbalanced across subjects. In the third experiment, subjects underwent two stages. In one stage subjects responded to stimuli drawn from the modular network, while in the other stage each subject was assigned a random k-4 network. The order of the two stages was counterbalanced. For each stage of each experiment, subjects responded to sequences of 1500 stimuli.

Experimental procedures. All participants provided informed consent in writing and experimental methods were approved by the Institutional Review Board of the University of Pennsylvania. In total, we recruited 363 unique participants to complete our studies on Amazon's Mechanical Turk: 106 completed just the first experiment, 102 completed just the second experiment, 71 completed both the first and second experiments in back-to-back stages, and 84 completed the third experiment. Worker IDs were used to exclude duplicate participants between experiments, and all participants were financially remunerated for their time. In the first two experiments, subjects were paid \$3-\$11 for up to an estimated 30-60 minutes: \$3 per network for up to two networks, \$2 per network for correctly responding on at least 90% of the trials, and \$1 for completing two stages. In the third experiment, subjects were paid up to \$9 for an estimated 60 minutes: \$5 for completing the experiment and \$2 for correctly responding on at least 90% of the trials on each stage.

Data analysis. To make inferences about subjects' internal expectations based upon their reaction times, we excluded all trials in which subjects responded incorrectly. We also excluded reaction times that were implausible, either three standard deviations from a subject's mean reaction time, below 100 ms, or over 3500 ms.

Measuring the effects of topology on reaction times. In order to estimate the effects of network topology on subjects' reaction times, one must overcome large inter-subject variability. To do so, we used linear mixed effects models, which have become prominent in human research where many measurements are made for each subject.[33] Compared with standard linear models, mixed effects models allow for differentiation between effects that are subject-specific and those that are representative of the prototypical individual in our experiments. Here, all models were fit using the `fitlme` function in MATLAB (R2018a), and random effects were chosen as the maximal structure that (i) allowed the model to converge and (ii) did not include effects whose 95% confidence intervals overlapped with zero. In what follows, when referring to our mixed effects models, we employ the standard R notation.

For the first experiment, in order to measure the impact of entropy on reaction times (Fig. 1c), we regressed out a number of biomechanical dependencies: (i) variability due to the different button combinations, (ii) the natural quickening of reactions with trial number, and (iii) the change in reaction times between stages. We also regressed out the effects of recency on subjects' reaction times. Specifically, we fit a mixed effects model with the formula 'RT $\sim \log(\text{Trial}) * \text{Stage} + \text{Target} + \text{Recency} + (1 + \log(\text{Trial}) * \text{Stage} + \text{Recency} \,|\, \text{ID})$', where RT is the reaction time, Trial is the trial number (it is common to consider $\log(\text{Trial})$ rather than the trial number itself[16,17]), Stage is the stage of the experiment, Target is the target button combination, Recency is the number of trials since the last instance of the current stimulus, and ID is each subject's unique ID.

For the second experiment, to measure differences in reaction times between transitions in the modular network (Fig. 1e), we fit a mixed effects model of the form 'RT $\sim \log(\text{Trial}) * \text{Stage} + \text{Target} + \text{Recency} + \text{Trans\_Type} + (1 + \log(\text{Trial}) * \text{Stage} + \text{Recency} \,|\, \text{ID})$', where Trans_Type is a dummy variable representing the type of transition (Fig. 1d) and the other variables are defined above. The three models for the three different comparisons are summarized in Tables S2-S4.

For the third experiment, to measure the difference in reaction times between the modular network and random k-4 networks (Fig. 1f), we fit a mixed effects model of the form 'RT $\sim \log(\text{Trial}) * \text{Stage} + \text{Target} + \text{Recency} + \text{Graph} + (1 + \log(\text{Trial}) * \text{Stage} + \text{Recency} \,|\, \text{ID})$', where Graph is a dummy variable representing the type of network (either modular or random k-4). This model is summarized in Table S5.

Estimating η values. Given a choice for the parameter η, and given a sequence of past nodes $x_1, \ldots, x_{t-1}$, the internal expectation of the next node x_t is predicted to be $\hat{P}_{x_{t-1},x_t}$. We predict subjects' reaction times $r(t)$ using the linear model $\hat{r}(t) = r_0 - r_1 \log \hat{P}_{x_{t-1},x_t}$, where $-\log \hat{P}_{x_{t-1},x_t}$ is the predicted perceived information at time t. Before estimating η, r_0, and r_1, we regress out subjects' biomechanical dependencies using the mixed effects model 'RT $\sim \log(\text{Trial}) * \text{Stage} + \text{Target} + \text{Recency} + (1 + \log(\text{Trial}) * \text{Stage} + \text{Recency} \,|\, \text{ID})$', where all variables are defined above. Then, to estimate the model parameters that best describe a subject's reactions, we minimize the root-mean-square error (RMSE) with respect to each subject's reaction times. We note that, given a choice for η, the linear

parameters r_0 and r_1 can be calculated analytically. Thus, the estimation problem can be restated as a one-dimensional minimization problem; that is, minimizing RMSE with respect to η. To find the global minimum, we began by calculating RMSE along 101 values for η between 0 and 1. Then, starting at the minimum value of this search, we performed gradient descent until the gradient $\frac{\partial \text{RMSE}}{\partial \eta}$ fell below an absolute value of 10^{-6}. The resulting distributions of model parameters over subjects are shown in Supplementary Fig. 1. For more details, see Supplementary Sec. 4.

Data Availability

The data that support the findings of this study are available from the corresponding author upon request.

Supplementary Information Supplementary text and figures accompany this paper.

Acknowledgements We thank Eric Horsley, Harang Ju, David Lydon-Staley, Shubhankar Patankar, Pragya Srivastava, and Erin Teich for feedback on earlier versions of the manuscript. We thank Dale Zhou for providing the code used to generate the language networks. D.S.B., C.W.L., and A.E.K. acknowledge support from the John D. and Catherine T. MacArthur Foundation, the Alfred P. Sloan Foundation, the ISI Foundation, the Paul G. Allen Family Foundation, the Army Research Laboratory (W911NF-10-2-0022), the Army Research Office (Bassett-W911NF-14-1-0679, Grafton-W911NF-16-1-0474, DCIST- W911NF-17-2-0181), the Office of Naval Research, the National Institute of Mental Health (2-R01-DC-009209-11, R01-MH112847, R01-MH107235, R21-M MH-106799), the National Institute of Child Health and Human Development (1R01HD086888-01), National Institute of Neurological Disorders and Stroke (R01 NS099348), and the National Science Foundation (BCS-1441502, BCS-1430087, NSF PHY-1554488 and BCS-1631550). L.P. is supported by an NSF Graduate Research Fellowship. The content is solely the responsibility of the authors and does not necessarily represent the official views of any of the funding agencies.

Author Contributions C.W.L. and D.S.B. conceived the project. C.W.L. designed the framework and performed the analysis. C.W.L. and A.E.K. performed the human experiments. C.W.L. wrote the manuscript and Supplementary Information. L.P., A.E.K., and D.S.B. edited the manuscript and Supplementary Information.

Competing Interests The authors declare no competing financial interests.

Corresponding Author Correspondence and requests for materials should be addressed to D.S.B. (dsb@seas.upenn.edu).

Supplementary Information

Human information processing in complex networks

1 Introduction

In this Supplementary Information, we provide extended analysis and discussion to support the results presented in the main text. In Sec. 2, we clarify the fundamental differences between our work and previous research on human information processing and complex networks. In Sec. 3, we give a brief introduction to information theory and provide explicit definitions for the quantities discussed in the main text. In Sec. 4, we introduce existing research studying how humans form expectations about complex transition networks. In Sec. 5, we present the effects of graph topology on human reaction times measured in our serial response experiments. We begin in Sec. 5 by demonstrating the impact of entropy on reaction times and then proceed to describe effects beyond entropy (Sec. 5, 5). In Sec. 6, we verify that our conclusions concerning the information properties of real networks hold for (i) various values of η (Sec. 6), (ii) different models of internal representations (Sec. 6), and (iii) directed versions of the real networks (Sec. 6). In Sec. 7, we derive analytic results for the entropies of various canonical network families. In Sec. 8, we derive a number of analytic results concerning the KL divergence between random walks and human expectations. In Sec. 9, we develop a generative model of hierarchically modular networks that combines the heterogeneity of scale-free networks with the community structure of stochastic block networks. Finally, in Sec. 10, the real networks analyzed in this work are listed and briefly described.

2 Previous work

Our work builds on a long record of research in information theory,[1,12] network science,[34,35] and cognitive science.[13,36,37] Here, we clarify the relationships and differences between our work and earlier research in these areas. In particular, we emphasize two main points:

1. In the study of complex networks, traditional definitions of network complexity focus on

the structure of a network itself.[2–5,34,35] While characterizing the inherent complexity of a network is a fascinating problem with numerous applications, many complex systems – from language and music to social networks and literature – exist for the sole purpose of communicating information with and between humans. Therefore, to fully understand the structure of these communication networks, one must consider the perspective of a human observer. In this work, we show that this shift in perspective from inherent complexity to perceived complexity can be formally defined using information theory and provides critical insights into the structure of real communication networks.

2. Significant research in cognitive science and statistical learning has studied how humans build internal expectations about the world around them,[13–16,36–38] generating deep insights about human learning and behavior. Building upon this work, we consider a complimentary problem that has received far less attention: Given a model of human expectations, what types of structures support efficient human communication? The answer to this question may shed light on the organization of real communication systems and help us to design new systems with desirable properties.

2.1 – Definitions of network entropy. Information theory has been linked with network science since its inception, when Shannon estimated the entropy rate of the English language by studying a random walk on the network of word transitions in a book.[1] Since then, information theory has been used extensively to characterize the structure and function of complex networks.[2–5,34,35,39–41] Of particular interest are ongoing efforts studying the entropies of random walks on complex networks. For example, the entropies of a number of canonical network families have been derived, including constant-degree networks[12] and power-law distributed networks.[3] Meanwhile, researchers have developed strategies for maximizing the entropy of random walks by tuning the edge weights in a network,[41–44] and it is now known that temporal regularities in random walks reveal key aspects of modularity and community structure.[2,39]

Our work extends these efforts by taking into account human expectations. Specifically, we consider the cross entropy (or perceived information) of random walks relative to human ex-

pectations, which can be broken down into network entropy (or produced information) and KL divergence (or the inefficiency of human expectations). Importantly, we discover that the entropy and KL divergence characterize distinct aspects of network structure: while entropy is driven by degree heterogeneity, the KL divergence is determined by a network's modular organization. Additionally, we provide a number of novel results concerning network entropy and KL divergence that may be of independent interest. These include analytic approximations for the entropies of networks with Poisson and exponential degree distributions as well as static model networks (see Supplementary Sec. 7) and the KL divergences of Erdös-Rényi and stochastic block networks (see Supplementary Sec. 8).

2.2 – Human information processing. Efforts to relate human cognition to information theory have a rich history, spanning the fields of cognitive science, psychology, and neuroscience. For example, information theory has been used to study linguistics,[6,8] decision-making,[9,45] Bayesian learning,[46] neural coding,[47] and vision.[48] In fact, the relativity of information – the notion that the amount of information conveyed by a message depends not just on the inherent complexity of the message, but also on the expectations of a receiver – was previously studied in linguistics to understand the dependence of meaning in language on context.[8] To quantify perceived information, however, one requires a mathematical model of human expectations.

Here, we employ recent models from cognitive science and statistical learning to quantitatively study perceived information. In particular, our experimental results build upon a long line of research in cognitive science linking human reaction times to information processing[10,49] as well as efforts in statistical learning investigating the relationship between human expectations and the network structure of probabilistic transitions.[13–17,36–38,50,51] Additionally, our analytical results leverage mathematical models of human expectations that have roots in temporal context and temporal difference learning[19,52] and also appear in reinforcement learning[18,53] and statistical learning.[15,17] Using these models of human expectations $\hat{P}$, we are able to quantify the amount of information $\langle -\log \hat{P} \rangle$ that a human perceives when observing a sequence of stimuli.

3 Perceived information

We introduce a specific definition for the information of a sequence of stimuli as perceived by a human observer. We assume that the sequence is generated according to a Markov process with transition probability matrix P. The amount of information produced by a transition from one stimulus i to another stimulus j is $-\log P_{ij}$.[1] To quantify the amount of information produced by the entire sequence (per stimulus), one averages this quantity over the Markov process,[12]

$$\langle -\log P_{ij} \rangle_P = -\sum_i \pi_i \sum_j P_{ij} \log P_{ij}, \tag{2}$$

where $\boldsymbol{\pi}$ is the stationary distribution defined by the stationary condition $\boldsymbol{\pi}^\intercal = \boldsymbol{\pi}^\intercal P$. The average quantity in Eq. (2) is known as the *entropy rate* of the sequence, although it is often referred to simply as the *entropy*, and it is denoted by $S(P)$.

While the entropy rate quantifies the amount of information produced by a sequence, we are interested in studying the amount of information that a human perceives when observing such a sequence. Consider a human observer with expectations based on an internal estimate of the transition probabilities $\hat{P}$. When observing a transition from one stimulus i to another stimulus j, the observer perceives $-\log \hat{P}_{ij}$ bits of information, which, when averaged over the Markov process, takes the form

$$\langle -\log \hat{P}_{ij} \rangle_P = -\sum_i \pi_i \sum_j P_{ij} \log \hat{P}_{ij}. \tag{3}$$

This quantity is the *cross entropy rate* (or simply the *cross entropy*) $S(P, \hat{P})$ between the Markov process P and the observer's expectations $\hat{P}$.

3.1 – Cross entropy. If the observer's expectations are exact (that is, if $\hat{P} = P$), then the cross entropy (Eq. (3)) reduces to the entropy (Eq. (2)); in other words, if the observer correctly anticipates the frequency of stimuli, then the amount of information they perceive equals the amount of information produced by the sequence itself. However, if the observer's expectations differ from reality (that is, if $\hat{P} \neq P$), then the observer perceives additional information. To see this relationship, we

consider the simple identity,

$$S(P, \hat{P}) = S(P) + D_{\text{KL}}(P||\hat{P}), \tag{4}$$

where $D_{\text{KL}}(P||\hat{P})$ is the Kullback-Leibler (KL) divergence between P and $\hat{P}$, defined by

$$D_{\text{KL}}(P||\hat{P}) = \langle -\log \frac{\hat{P}_{ij}}{\hat{P}_{ij}} \rangle_P = -\sum_i \pi_i \sum_j P_{ij} \log \frac{\hat{P}_{ij}}{P_{ij}}. \tag{5}$$

Gibbs' inequality[12] states that $D_{\text{KL}}(P||\hat{P}) \geq 0$ for all P and $\hat{P}$, and that $D_{\text{KL}}(P||\hat{P}) = 0$ only if $\hat{P} = P$. Therefore, we see that the perceived information (or cross entropy) is lower-bounded by the produced information (or entropy).

3.2 – Random walks on a network. Every stationary Markov process is equivalent to a random walk on an underlying (possibly weighted, directed) network, where each state is encoded as a node in the network. Specifically, given a transition probability matrix P, one can choose an adjacency matrix G such that

$$P_{ij} = \frac{1}{k_i^{\text{out}}} G_{ij}, \tag{6}$$

where $k_i^{\text{out}} = \sum_j G_{ij}$ is the out-degree of node i. To develop a number of analytic results, we briefly consider the special case of an undirected network. In this case, the out-degree of a node i is referred to simply as its degree k_i. If G is connected, then there exists a unique stationary distribution over nodes, and it is proportional to the degree vector, such that $\boldsymbol{\pi} = \frac{1}{2E}\boldsymbol{k}$, where $E = \frac{1}{2}\sum_{ij} G_{ij}$ is the number of edges in the network. Therefore, for random walks on a connected, undirected network, we find that the cross entropy can be written as

$$S(P, \hat{P}) = -\frac{1}{2E} \sum_{ij} G_{ij} \log \hat{P}_{ij}, \tag{7}$$

reflecting a weighted average of $-\log \hat{P}_{ij}$ over the edges in the network. Moreover, if we further restrict our focus to unweighted networks, then the entropy takes a particularly simple form:[3]

$$S(P) = \frac{1}{2E} \sum_i k_i \log k_i. \tag{8}$$

In this case, it is clear that the entropy of a random walk is uniquely defined by the degree sequence of the network,[12] a result that is verified numerically for real networks in Fig. 2d.

4 Human expectations

When observing sequences of stimuli, humans constantly rely on their internal estimate of the transition structure to anticipate what is coming next.[49,54–57] Indeed, building expectations about probabilistic relationships allows humans to perform abstract reasoning,[58] produce language,[59] develop social intuition,[60,61] and segment streams of stimuli into self-similar parcels.[62] Moreover, as discussed above, a person's internal expectations, defined by the estimated transition probability matrix $\hat{P}$, determine the amount of information $S(P, \hat{P})$ that they receive from a transition structure defined by P. To study the cross entropy $S(P, \hat{P})$, we require a model $\hat{P} = f(P)$ of how humans internally estimate transition structures in the world around them.

4.1 – Temporal integration of stimuli. Models describing how humans learn and estimate transition structures typically stem from Bayesian inference[60,63,64] or notions of hierarchical learning.[14,36,38,65] A common thread across many models is that humans relate stimuli that are not directly adjacent in time.[15,54] These non-adjacent relationships have been hypothesized to reflect planning for the future,[19,53] context-dependent memory effects,[52,66] and even errors in optimal Bayesian learning.[17] Independent of the underlying mechanisms, the fact that humans relate non-adjacent stimuli results in a common functional form for the expectations $\hat{P}$ where the true transition structure P is integrated over time. Mathematically, this means that $\hat{P}$ includes higher powers of P:

$$\hat{P} = C(g(1)P + g(2)P^2 + \ldots) = C\sum_{t=1}^{\infty} g(t)P^t, \tag{9}$$

with progressively higher powers downweighted by a decreasing function $g(t) \geq 0$, where $C = (\sum_{t=1}^{\infty} g(t))^{-1}$ is a normalization constant.

There exist a number of simple choices for the function $g(t)$. For example, if people's integration of the transition structure drops off as a power law, then we have $g(t) = t^{-\alpha}$ with power-law exponent $\alpha > 1$. Instead, if the integration drops off with the factorial of t (that is, if $g(t) = 1/t!$), then $\hat{P} = (e^P - I)/(e - 1)$, where e^P is the matrix exponential, which is closely related to the communicability of P from graph theory.[67] In Sec. 6 we study the information properties of real networks under these alternative representation models, finding qualitatively the same results as

those described in the main text.

4.2 – Exponential model. Throughout the main text, we focus on a specific model for $\hat{P}$ in which the integration of the transition structure drops off exponentially, such that $g(t) = \eta^{t-1}$, where $\eta \in (0, 1)$ is the integration constant. This model is closely related to the successor representation from reinforcement learning,[18,53] which can be derived from temporal context and temporal difference learning,[19] and can independently be shown to arise from errors in human cognition.[17] The model takes a concise analytic form,

$$\hat{P} = (1 - \eta)P(I - \eta P)^{-1}. \tag{10}$$

In the limit $\eta \to 0$, we see that $\hat{P} \to P$, and hence the estimate becomes equivalent to the true transition structure P (Fig. S1a). By contrast, in the limit $\eta \to 1$, we find that $\hat{P} \to \mathbf{1}\boldsymbol{\pi}^{\intercal}$, where $\mathbf{1}$ is the vector of all ones and $\boldsymbol{\pi}$ is the stationary distribution, such that the expectations lose all resemblance to the true structure (Fig. S1a). For intermediate values of η, higher-order features of the network, such as communities of densely-connected nodes, maintain much of their probability weight, while some of the fine-scale features, like the edges between communities, fade away (Fig. S1a). This strengthening of expectations for transitions within communities relative to transitions between communities is precisely the effect we observe in human reaction times (Fig. 1e).

In order to make quantitative predictions for the KL divergence $D_{\text{KL}}(P||\hat{P})$, it is useful to have an estimate for the integration parameter η based on real human data. We estimate η by making predictions for subjects' reaction times and then minimizing the prediction error with respect to η. Given a sequence of nodes $x_1, \ldots, x_{t-1}$, we note that the reaction to the next node x_t is determined by the perceived information of the transition from x_{t-1} to x_t, with expectations calculated at time $t - 1$. Formally, this perceived information is given by $-\log \hat{P}_{x_{t-1},x_t}$, and we make the following linear prediction for the reaction time,

$$\hat{r}(t) = r_0 - r_1 \log \hat{P}_{x_{t-1},x_t}, \tag{11}$$

where the intercept r_0 represents a person's minimum average reaction time (with perfect anticipation of the next stimulus, $\hat{P}_{x_{t-1},x_t} = 1$) and the slope r_1 quantifies the strength of the relationship between a person's reactions and their perceived information, measured in units of time per bit.

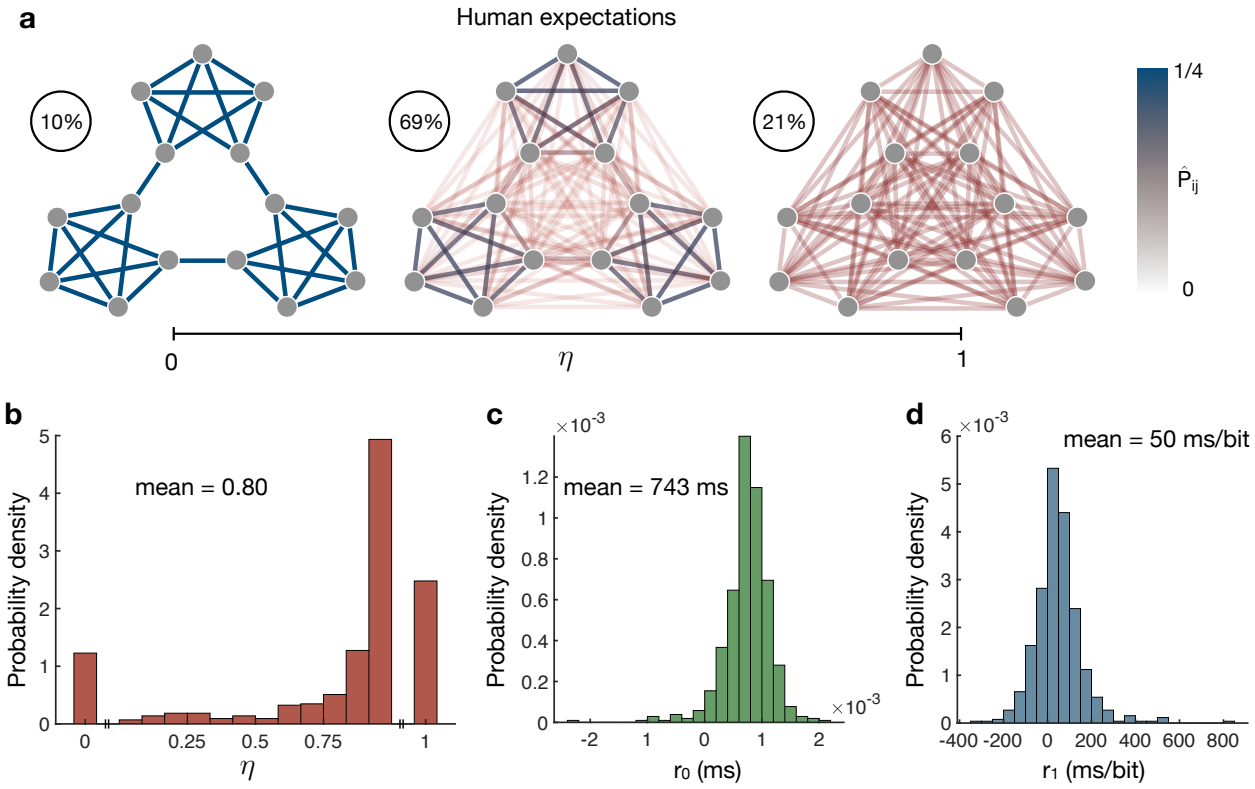

Fig. S1 | Estimated model parameters relating human expectations to reaction times.

a, Human expectations $\hat{P}$ for the modular network. For $\eta \to 0$, expectations become exact (left; 10% of subjects), while for $\eta \to 1$, expectations become all-to-all, losing any resemblance to the true structure (right; 21% of subjects). At intermediate values of η, the communities maintain probability weight, while expectations for between-community transitions weaken (center; 69% of subjects). **b**-**d**, Distributions of model parameters estimated from subjects' reaction times. Distributions are over all 518 completed sequences. For the integration parameter η (**b**), 53 subjects were best described as having exact representations ($\eta \to 0$) and 107 lacked any notion of the transition structure ($\eta \to 1$), while across all subjects the average value was $\eta = 0.80$. The intercept r_0 is mostly positive (**b**), with an average value of 743 ms. The slope r_1 is also mostly positive (**d**), with an average value of 50 ms/bit.

Before estimating the model parameters, we first regress out the dependencies of each subject's reaction times on the button combinations, trial number, experimental stage, and recency using a mixed effects model of the form '$RT \sim \log(Trial) * Stage + Target + Recency + (1 + \log(Trial) * Stage + Recency \,|\, ID)$', where RT is the reaction time, $Trial$ is the trial number between 1 and

1500 (we found that $\log(Trial)$ was far more predictive of subjects' reaction times than the trial number itself), $Stage$ is the stage of the experiment (either one or two), $Target$ is the target button combination, $Recency$ is the number of trials since the last instance of the current stimulus, and ID is each subject's unique ID. Then, to estimate the parameters η, r_0, and r_1 that best describe a subjects' reaction times, we minimize the RMS error $\sqrt{\frac{1}{T}\sum_t (r(t) - \hat{r}(t))^2}$, where $r(t)$ is the reaction time on trial t after regressing out the above dependencies and T is the number of trials in the experiment. The distributions of the estimated parameters are shown in Fig. S1b-d. Among the 518 completed sequences (across 363 unique subjects), 53 were best described as having expectations that exactly matched the transition structure ($\eta \to 0$) and 107 seemed to lack any notion of the transition structure whatsoever ($\eta \to 1$), with an overall average value of $\eta = 0.80$.

Equipped with the model of human expectations in Eq. (10), we can make quantitative predictions for the perceived information of different transition structures. For example, considering the three types of transitions in the modular network (Fig. S2a), we find across all values of η that the perceived information $-\log \hat{P}_{ij}$ is highest for transitions between communities, followed by transitions at the boundaries of communities, and lowest for transitions deep within communities (Fig. S2b). This prediction precisely matches the variations in reaction times for the different transitions observed in our human experiments (Fig. 1e). Furthermore, we find that the average perceived information (or cross entropy) $\langle -\log \hat{P}_{ij} \rangle_P$ is lower in the modular network than almost any other network of the same entropy across all values of η (Fig. S2c). This final prediction explains the observed decrease in reaction times in the modular network relative to random entropy-preserving networks (Fig. 1f).

5 Reaction time effects

In order to directly probe the information that humans perceive, we employ an experimental framework recently developed in statistical learning.[15–17,50,51] Specifically, we present human subjects with sequences of stimuli on a computer screen, each stimulus depicting a row of five grey squares with one or two of the squares highlighted in red (Fig. 1a, left). In response to each stimulus, sub-

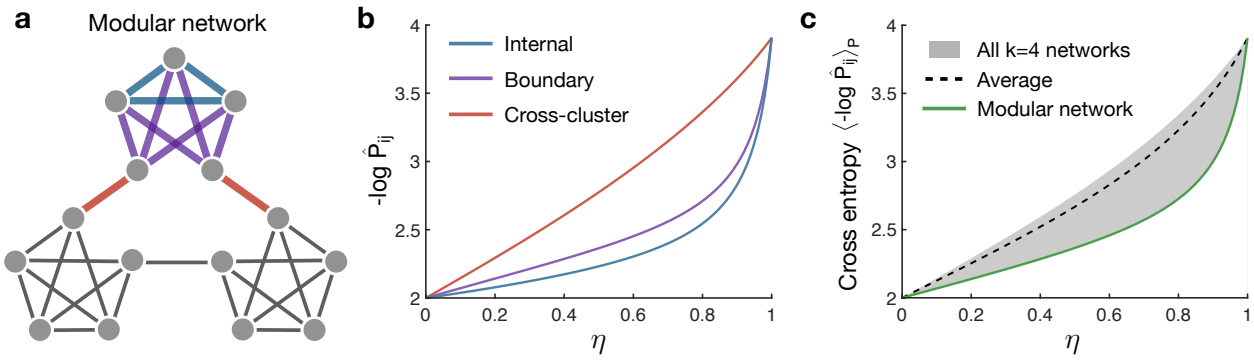

Fig. S2 | Network effects on human reaction times beyond entropy.

a, Modular network with three modules of five nodes each. By symmetry the network contains three distinct types of edges: those deep within communities (blue), those at the boundaries of communities (purple), and those between communities (red). **b**, Perceived information $-\log \hat{P}_{ij}$ for the three edge types as a function of η. Across all values of η, the perceived information is highest for cross-cluster edges, followed by boundary edges, and lowest for internal edges, thus explaining the observed differences in human reaction times (Fig. 1e). **c**, Cross entropy (or network-averaged perceived information) $\langle -\log \hat{P}_{ij} \rangle_P$ as a function of η for the modular network (green) and all k-4 networks (the grey region denotes the range and the dashed line denotes the mean). The modular network maintains nearly the lowest cross entropy among k-4 networks across all values of η, thereby explaining the overall decrease in reaction times in the modular network relative to random k-4 networks (Fig. 1f).

jects are asked to press one or two computer keys mirroring the highlighted squares (Fig. 1a, right). Each of the 15 different stimuli represents a node in an underlying transition network, upon which a random walk stipulates the sequential order of stimuli (Fig. 1b). By measuring the speed with which a subject responds to each stimulus, we can infer how much information they are processing – a fast reaction reflects an unsurprising (or uninformative) transition, while a slow reaction reflects a surprising (or informative) transition.[10,16,17,49,55,68]

In order to extract the effects of network structure on subjects' reaction times, we use linear mixed effects models, which have become prominent in human research where many measurements are made for each subject.[33,69] To fit our mixed effects models and to estimate the statistical significance of each effect we use the `fitlme` function in MATLAB (R2018a). In what follows,

when referring to our mixed effects models, we adopt the standard R notation.[70]

5.1 – Entropic effect. We first investigate the effect of entropy on subjects' reaction times. For undirected and unweighted networks, the entropy of a single transition from a node i to one of i's neighbors is $\log k_i$, where k_i is the degree of node i. To study a range of entropies, we consider completely random networks in which the node degrees are allowed to vary (specifically, we consider random networks with $N = 15$ nodes and $E = 30$ edges). We regress out the dependencies of each subject's reaction times on the button combinations, trial number, experimental stage, and recency using a mixed effects model with the formula '$RT \sim \log(Trial) * Stage + Target + Recency + (1 + \log(Trial) * Stage + Recency \mid ID)$', where RT is the reaction time, $Trial$ is the trial number between 1 and 1500, $Stage$ is the stage of the experiment (either one or two), $Target$ is the target button combination, $Recency$ is the number of trials since last observing a node,[71] and ID is each subject's unique ID. After regressing out these biomechanical dependencies, we find that subjects' average reaction times following nodes of a given degree are accurately predicted by the entropy (Fig. 1c), with a Pearson correlation of $r_p = 0.99$ ($p < 0.001$) and a slope of 32 ms/bit.

Additionally, to take into account variations in subjects' reaction times rather than simply studying average reaction times, we employ a mixed effects model of the form '$RT \sim \log(Trial) * Stage + Target + Recency + Entropy + (1 + \log(Trial) * Stage + Recency + Entropy \mid ID)$', where $Entropy$ is the logarithm of the degree of the preceding node. The mixed effects model is summarized in Table S1, reporting a 26 ms increase in reaction times for each additional bit of information. We remark that this bit rate is close to that estimated from subjects' average reaction times in random graphs (32 ms/bit; Fig. 1c) and is also comparable to the bit rate estimated from our linear prediction of subjects' reaction times in constant-degree graphs (50 ms/bit; Fig. S1d).

5.2 – Extended cross-cluster effect. We next investigate reaction time patterns that are driven by perceived information beyond entropy. To experimentally control for the entropy of transitions, we focus on networks of constant degree 4 ($N = 15$ and $E = 30$). Specifically, we consider the modular network shown in Fig. S2a, consisting of three communities or clusters comprised of five nodes each. Recent research has shown that people can detect transitions be-

Effect	Estimate (ms)	t-value	Pr(>|t|)	Significance
(Intercept)	1324.8 ± 49.6	26.73	< 0.001	$***$
log(Trial)	-89.6 ± 5.8	-15.41	< 0.001	$***$
Stage	-538.9 ± 54.1	-9.96	< 0.001	$***$
Recency	1.9 ± 0.1	21.63	< 0.001	$***$
Entropy	26.1 ± 4.1	6.39	< 0.001	$***$
log(Trial):Stage	78.2 ± 6.6	11.91	< 0.001	$***$

Table S1 | Mixed effects model measuring the effect of entropy on human reaction times. We find a significant 26 ms increase in reaction times for each additional bit of entropy (grey). All effects are significant with p-values less than 0.001 ($***$).

tween the clusters[15] and that between-cluster transitions yield increases in reaction times relative to within-cluster transitions.[16,17] These behaviors are surprising in light of the fact that all edges in the network have identical transition probabilities and therefore identical entropy. Here, we extend these results to include all three of the distinct types of transitions in the modular network (Fig. S2a): those deep within communities (internal transitions), those at the boundaries of communities (boundary transitions), and those between communities (between-cluster transitions).

We use a mixed effects model with the formula '$RT \sim \log(Trial) * Stage + Target + Recency + Trans\_Type(1 + \log(Trial) * Stage + Recency \,|\, ID)$', where $Trans\_Type$ represents the type of transition (either internal, boundary, or cross-cluster). We find a 39 ms increase in reaction times for between-cluster transitions relative to internal transitions within clusters (Table S2), a 31 ms increase in reaction times for between-cluster transitions relative to boundary transitions within clusters (Table S3), and a 7 ms increase in reaction times for boundary transitions relative to internal transitions within clusters (Table S4). Notably, this hierarchy of reaction times is the same as that predicted by our cross entropy framework (Fig. S2b).

Effect	Estimate (ms)	t-value	Pr($>$|t|)	Significance
(Intercept)	1365.6 ± 46.8	29.15	< 0.001	$***$
log(Trial)	-86.9 ± 5.2	-16.75	< 0.001	$***$
Stage	-549.2 ± 52.9	-10.38	< 0.001	$***$
Recency	1.5 ± 0.1	18.40	< 0.001	$***$
Trans_Type	38.69 ± 2.3	16.99	< 0.001	$***$
log(Trial):Stage	63.5 ± 5.8	11.01	< 0.001	$***$

Table S2 | Mixed effects model measuring the difference in reaction times between internal and between-cluster transitions. We find a significant 39 ms increase in reaction times for between-cluster transitions relative to internal transitions within communities (grey). All effects are significant with p-values less than 0.001 ($***$).

Effect	Estimate (ms)	t-value	Pr($>$|t|)	Significance
(Intercept)	1349.3 ± 45.8	29.48	< 0.001	$***$
log(Trial)	-86.0 ± 5.2	-16.39	< 0.001	$***$
Stage	-495.41 ± 49.6	-9.98	< 0.001	$***$
Recency	1.6 ± 0.1	23.28	< 0.001	$***$
Trans_Type	30.8 ± 2.1	14.50	< 0.001	$***$
log(Trial):Stage	62.1 ± 5.8	10.76	< 0.001	$***$

Table S3 | Mixed effects model measuring the difference in reaction times between boundary and between-cluster transitions. We find a significant 31 ms increase in reaction times for between-cluster transitions relative to boundary transitions within communities (grey). All effects are significant with p-values less than 0.001 ($***$).

5.3 – Modular effect. We finally investigate the effects of perceived information averaged over all transitions in a network, defined by the cross entropy in Eq. (3). To do so, we compare reaction

Effect	Estimate (ms)	t-value	Pr($>$|t|)	Significance
(Intercept)	1333.3 ± 44.3	30.13	< 0.001	$***$
log(Trial)	-84.0 ± 4.9	-17.11	< 0.001	$***$
Stage	-464.8 ± 47.2	-9.84	< 0.001	$***$
Recency	1.5 ± 0.1	24.55	< 0.001	$***$
Trans_Type	6.6 ± 1.3	4.96	< 0.001	$***$
log(Trial):Stage	60.0 ± 5.4	11.12	< 0.001	$***$

Table S4 | Mixed effects model measuring the difference in reaction times between internal and boundary transitions within clusters. We find a significant 7 ms increase in reaction times for boundary transitions relative to internal transitions within communities (grey). All effects are significant with p-values less than 0.001 ($***$).

times in the modular network with reaction times in random k-4 networks. We remark that the entropy (defined in Eq. (2)) is identical across all graphs considered. We use a mixed effects model of the form '$RT \sim \log(Trial) * Stage + Target + Recency + Network\_Type(1 + \log(Trial) * Stage + Recency \,|\, ID)$', where $Network\_Type$ represents the type of network (either modular of random k-4). The estimated mixed effects model is summarized in Table S5, reporting a 24 ms increase in reaction times for random degree-preserving networks relative to the modular network. Notably, this effect is predicted by our cross entropy framework (Fig. S2c). Moreover, this result provides direct evidence that, even after controlling for the entropy of a network, modular structure reduces the total amount of information that humans perceive when observing a sequence of stimuli.

6 Real networks

In the main text, we show that real networks exhibit two consistent information properties: they have high entropy and low KL divergence from human expectations. When calculating the KL divergence, we use the model $\hat{P}$ defined in Eq. (10) with η set to the average value from our human

Effect	Estimate (ms)	t-value	Pr($>$|t|)	Significance
(Intercept)	1195.0 ± 48.8	24.49	< 0.001	$***$
log(Trial)	-71.9 ± 4.9	-14.61	< 0.001	$***$
Stage	-405.3 ± 36.9	-10.98	< 0.001	$***$
Recency	1.7 ± 0.1	19.65	< 0.001	$***$
Network_Type	23.5 ± 6.9	3.39	< 0.001	$***$
log(Trial):Stage	49.0 ± 5.1	9.61	< 0.001	$***$

Table S5 | Mixed effects model measuring the difference in reaction times between the modular network and random entropy-preserving networks. We find a significant 24 ms increase in reaction times for random entropy-preserving networks (that is, networks of constant degree 4) relative to the modular network (grey). All effects are significant with p-values less than 0.001 ($***$).

experiments (Fig. S1b). Additionally, in order to draw on our analytical results (see Supplementary Secs. 7 and 8), we focused on undirected versions of the real networks. Here, we show that the central conclusions in the main text concerning the information properties of real networks are robust to variations in these choices. Specifically, we verify that the KL divergence of real networks remains low for different values of η and different models for $\hat{P}$ altogether, and we confirm that the entropy remains high and the KL divergence remains low for directed versions of the real networks.

6.1 – Varying η. We first investigate how the KL divergence varies as a function of the inaccuracy parameter η. To recall, the KL divergence, defined in Eq. (5), represents the inefficiency due to a person's expectations $\hat{P}$. We consider the model of expectations used in the main text, $\hat{P} = (1-\eta)P(I-\eta P)^{-1}$, while varying the parameter η between zero and one. We find that all of the real networks considered maintain a lower KL divergence than fully randomized versions of the networks across all values of η (Fig. S3a). In the limit $\eta \to 0$, the KL divergence of both real and randomized networks tends toward zero (Fig. S3a), as expected. As η increases, the difference in efficiency between the real and fully randomized networks grows (Fig. S3b). We also

generate randomized versions of the real networks that maintain identical entropies by preserving the degree distribution. Even when compared against random networks with the same entropy, all of the real networks attain lower KL divergence across all values of η (Fig. S3c). Just as for the fully randomized networks, the difference in efficiency between real and entropy-preserving random networks grows as η increases (Fig. S3d). These results confirm that our conclusions in the main text are robust to variations in the inaccuracy parameter η.

6.2 – Different internal representations. Here, we study the KL divergence for different models of the human expectations $\hat{P}$. First, we consider the power-law model, defined by Eq. (9) with integration function $g(t) = t^{-\alpha}$, where $\alpha \in (1, \infty)$ is the single parameter. Varying α between 1 and 10, we find that all of the real networks display lower KL divergence than fully randomized versions for all values of α (Fig. S4a). Moreover, this difference in efficiency grows as α decreases (Fig. S4b); that is, the difference in KL divergence increases as the expectations $\hat{P}$ integrate over longer time scales, which is analogous to η increasing. Even when compared with random versions that preserve the entropy, the real networks still exhibit lower KL divergence across all values of α (Fig. S4c,d).

Second, we consider the factorial model for $\hat{P}$, defined by Eq. (9) with integration function $g(t) = 1/t!$. As discussed in Supplementary Sec. 4.1, this model takes the analytic form $\hat{P} = (e^P - I)/(e - 1)$, where e^P is the matrix exponential. Calculating the KL divergence, we find qualitatively the same results as for the previous two models. Namely, when compared against both fully randomized and entropy-preserving (i.e., degree-preserving) randomized versions, all of the real networks studied maintain a lower KL divergence (Fig. S5). Taken together, the results of this and the previous subsections indicate that the low KL divergence observed in real networks is robust to different choices for the specific model of human expectations.

6.3 – Directed networks. We now consider directed versions of the real networks. Among the 40 networks chosen for analysis, 28 have directed versions (see Table S6). Analysis of directed networks follows in much the same way as our previous analysis of undirected networks; the only difference is that, when computing the entropy (Eq. 2) and KL divergence (Eq. 5), we calculate

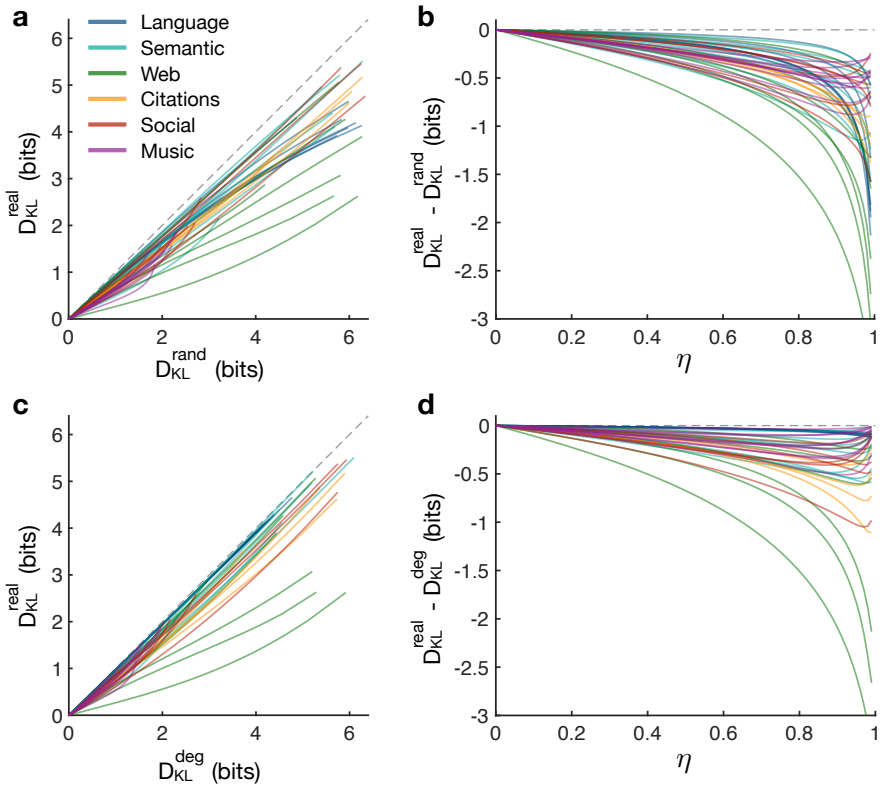

Fig. S3 | KL divergence of real networks for different values of η.

a, KL divergence of fully randomized versions of the real networks listed in Table S6 ($D_{\text{KL}}^{\text{rand}}$) compared with the true value ($D_{\text{KL}}^{\text{real}}$) as η varies from zero to one. Every real networks maintains lower KL divergence than the corresponding randomized network across all values of η. **b**, Difference between the KL divergence of real and fully randomized networks as a function of η. **c**, KL divergence of degree-preserving randomized versions of the real networks ($D_{\text{KL}}^{\text{deg}}$) compared with $D_{\text{KL}}^{\text{real}}$ as η varies from zero to one. The real networks display lower KL divergence than the degree-preserving randomized versions across all values of η. **d**, Difference between the KL divergence of real and degree-preserving randomized networks as a function of η. All networks are undirected, and each line is calculated using one randomization of the corresponding real network.

the stationary distribution $\boldsymbol{\pi}$ numerically by solving the eigenvector equation $\boldsymbol{\pi}^{\intercal} = \boldsymbol{\pi}^{\intercal} P$. We find that most of the directed real networks have higher entropy than completely randomized versions (Fig. S6a); the main exceptions are the citation networks, which we discuss in further detail below. We also find that all of the directed real networks have lower KL divergence than completely ran-

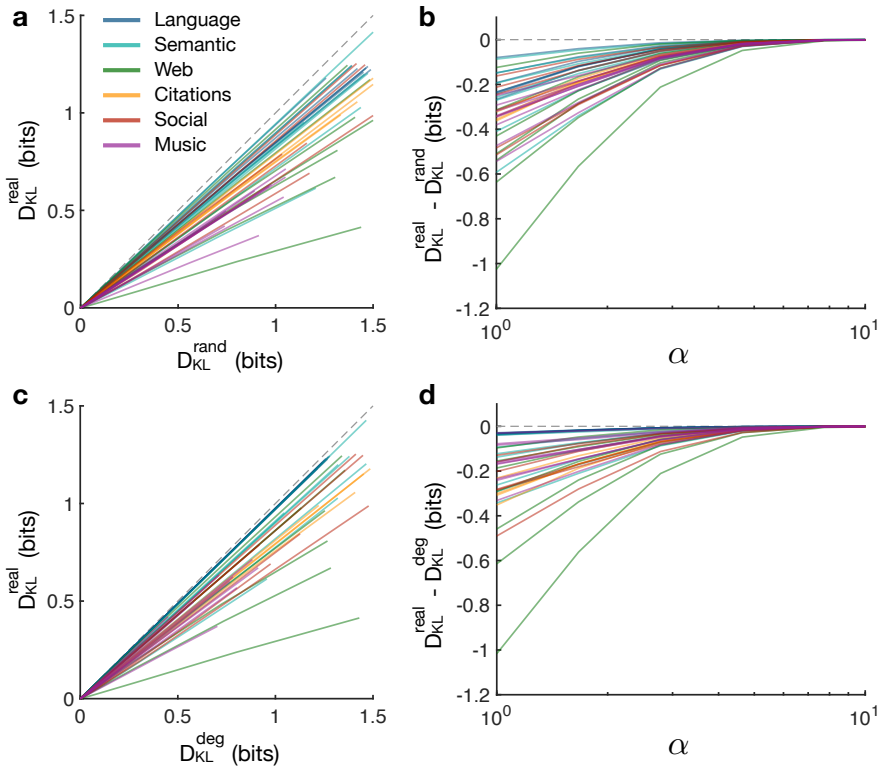

Fig. S4 | KL divergence of real networks under the power-law model of human expectations.

a, KL divergence of fully randomized versions of the real networks listed in Table S6 ($D_{\text{KL}}^{\text{rand}}$) compared with the true value ($D_{\text{KL}}^{\text{real}}$). Expectations $\hat{P}$ are defined as in Eq. (9) with $g(t) = t^{-\alpha}$, and we allow α to vary between 1 and 10. The real networks maintain lower KL divergence than the randomized network across all values of α. **b**, Difference between the KL divergence of real and fully randomized networks as a function of α. **c**, KL divergence of degree-preserving randomized versions of the real networks ($D_{\text{KL}}^{\text{deg}}$) compared with $D_{\text{KL}}^{\text{real}}$ as α varies from 1 to 10. The real networks display lower KL divergence than the degree-preserving randomized versions across all values of α. **d**, Difference between the KL divergence of real and degree-preserving randomized networks as a function of α. All networks are undirected, and each line is calculated using one randomization of the corresponding real network.

domized versions (Fig. S6b), where the expectations $\hat{P}$ are calculated using the model in Eq. (10). If we instead compare against randomized versions that preserve both the in- and out-degrees of nodes, we see that the entropy of real networks remains relatively unchanged (Fig. S6c); again, the citation networks as a group represent the strongest exception to this result. Even when compared

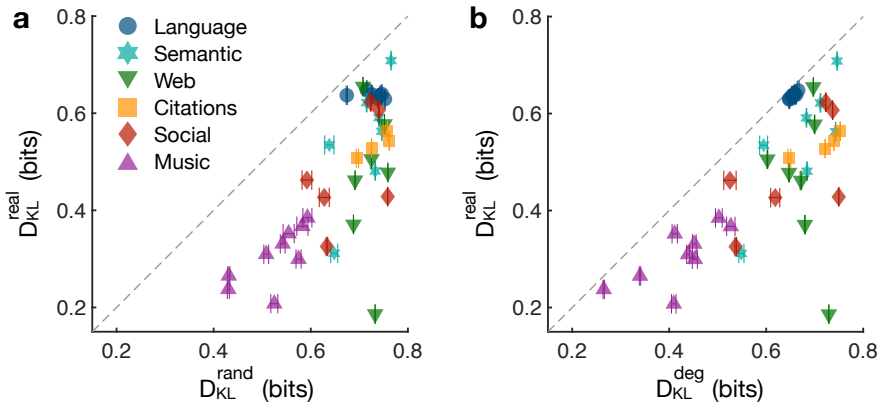

Fig. S5 | KL divergence of real networks under the factorial model of human expectations.

a, KL divergence of fully randomized versions of the real networks listed in Table S6 ($D_{\text{KL}}^{\text{rand}}$) compared with the exact value ($D_{\text{KL}}^{\text{real}}$). Expectations $\hat{P}$ are defined as in Eq. (9) with $g(t) = 1/t!$. **b**, KL divergence of degree-preserving randomized versions of the real networks ($D_{\text{KL}}^{\text{deg}}$) compared with $D_{\text{KL}}^{\text{real}}$. In both cases, the real networks maintain lower KL divergence than the randomized versions. Data points and error bars (standard deviations) are estimated from 10 realizations of the randomized networks.

with degree-preserving randomized versions, all of the directed real networks attain a lower KL divergence (Fig. S6d). Generally, these results demonstrate that our conclusions regarding the information properties of real networks also apply to directed networks: (i) their entropy is higher than completely randomized versions and is primarily driven by the degree distribution, and (ii) their KL divergence is lower than both completely randomized and degree-preserving randomized versions.

In the above analysis, we found that the directed versions of citation networks have lower entropy than randomized versions (Fig. S6a,c), directly contradicting the more general result that real communication networks have high entropy. Here we show that this contradiction stems from the inherently temporal nature of citation networks; namely, the fact that directed edges tend to flow backwards in time as more recent papers cite older papers. This temporal feature causes newer papers to have a lower in-degree than older papers, thereby disrupting the natural correlation between in- and out-degree in other real networks. For example, we see in the arXiv Hep-Th

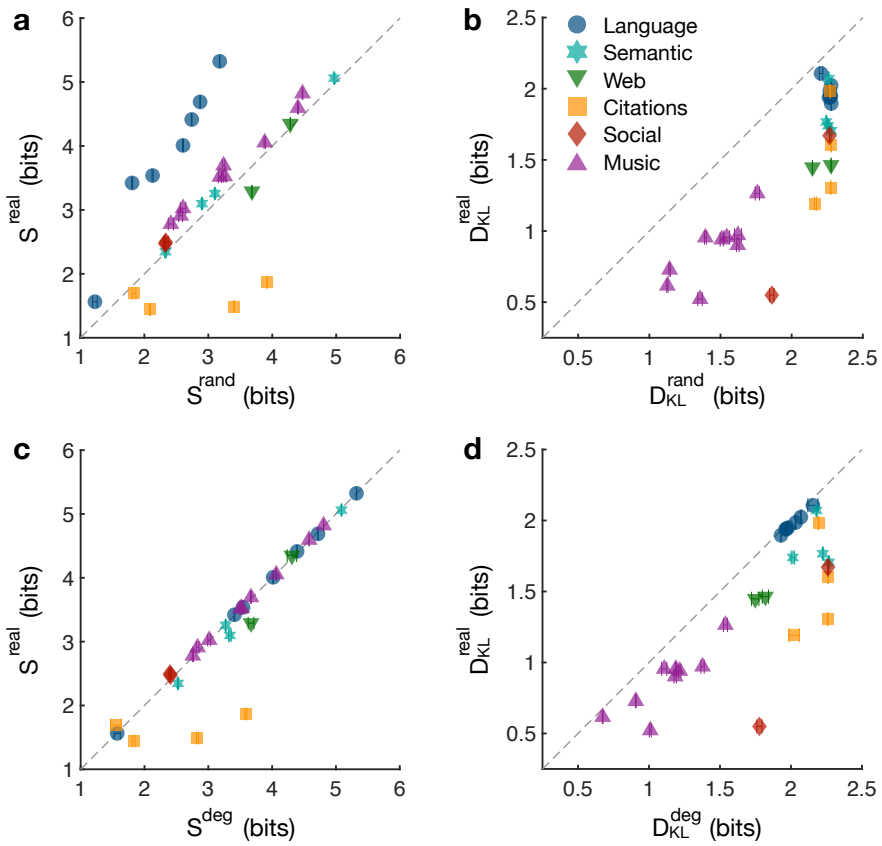

Fig. S6 | Entropy and KL divergence of directed versions of real networks.

a, Entropy of directed versions of the real networks listed in Table S6 (S^{real}) compared with fully randomized versions (S^{rand}). Entropy is calculated directly from Eq. (2) with the stationary distribution $\boldsymbol{\pi}$ calculated numerically. **b** KL divergence of directed versions of the real networks ($D_{\text{KL}}^{\text{real}}$) compared with fully randomized versions $D_{\text{KL}}^{\text{rand}}$. Expectations $\hat{P}$ are defined as in Eq. (10) with η set to the average value 0.80 from our human experiments. **c**, Entropy of randomized versions of directed real networks with in- and out-degrees preserved (S^{deg}) compared with S^{real}. **d**, KL divergence of degree-preserving randomized versions of directed real networks ($D_{\text{KL}}^{\text{deg}}$) compared with $D_{\text{KL}}^{\text{real}}$. Data points and error bars (standard deviations) are estimated from 100 realizations of the randomized networks.

citation network that the in- and out-degrees are only weakly correlated (Fig. S7a), while for the Shakespeare language network, the in- and out-degrees are tightly correlated (Fig. S7b). Since the in-degree of a node i roughly corresponds to the frequency with which random walks visit i, we can think of the in-degrees $\boldsymbol{k}^{\text{in}}$ as approximately determining the stationary distribution $\boldsymbol{\pi}$. By

contrast, the node-level entropy $S_i = -\sum_j P_{ij} \log P_{ij}$ is determined by the out-degree of node i, since $P_{ij} = \frac{1}{k_i^{\text{out}}} G_{ij}$ from Eq. (6). Since the network-averaged entropy is simply an inner product of the stationary distribution and the node-level entropy, $S = \sum_i \pi_i S_i$, this quantity is maximized in networks for which π_i and S_i are correlated. Returning to our previous examples, we find that the stationary distribution and node-level entropy are weakly negatively correlated in the citation network (Fig. S7c), whereas in the language network, the stationary distribution and node entropy are tightly correlated (Fig. S7d). We conclude that the apparent contradiction between directed citation networks and our general result that real networks have high entropy is primarily driven by the temporal nature of directed edges in citation networks. Indeed, if one instead allows random walks to flow along either direction of the edges, as in the undirected versions studied in the main text, we find that citation networks do have high entropy (Fig. 2a).

7 Entropy of random walks

Given the high entropy and low KL divergence from human expectations observed in real networks, it is natural to wonder what topological features give rise to these properties. We note that there has been a large amount of recent research studying maximum entropy random walks, wherein the topology of the network is fixed but the edge weights are tuned to maximize the entropy rate.[41–44] By contrast, here we are interested in understanding how, for fixed edge weights, different network topologies either increase or decrease the entropy of random walks.

To make analytic progress, we focus on unweighted, undirected networks. In this case, Eq. (8) shows that the entropy is determined by the degree sequence of the network. If we consider a random network ensemble with node degrees independently distributed according to a degree distribution $\mathcal{P}(k)$, then the average entropy rate is given by[3]

$$\begin{aligned} \langle S \rangle &= \frac{1}{2E} \sum_i \langle k_i \log k_i \rangle \\ &= \frac{\langle k \log k \rangle}{\langle k \rangle}, \end{aligned} \tag{12}$$

where the averages are taken over $\mathcal{P}(k)$.

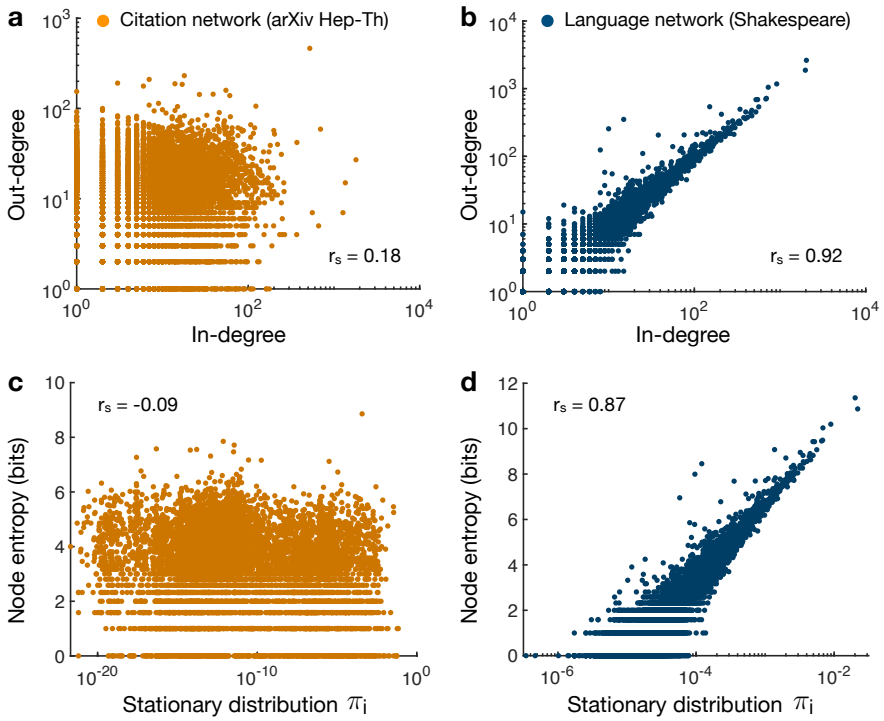

Fig. S7 | Comparison of directed citation and language networks.

a, Out-degrees $k_i^{\text{out}} = \sum_j G_{ij}$ of nodes in the arXiv Hep-Th citation network compared with the in-degrees $k_i^{\text{in}} = \sum_j G_{ji}$ of the same nodes; we find a weak Spearman's correlation of $r_s = 0.18$. **b**, Out-degrees compared with in-degrees of nodes in the Shakespeare language (word transition) network; we find a strong correlation $r_s = 0.92$. **c**, Entries in the stationary distribution π_i for different nodes in the citation network compared with the node-level entropy S_i; we find a weakly negative correlation $r_s = -0.09$. **d**, Entries in the stationary distribution compared with node-level entropies in the language network; we find a strong correlation $r_s = 0.87$.

7.1 – High-degree expansion. Since $k \log k$ is convex in k, it is clear that $\langle k \log k \rangle \geq \langle k \rangle \log \langle k \rangle$, and we arrive at a simple lower bound for the entropy,

$$\langle S \rangle \geq \log \langle k \rangle. \tag{13}$$

In fact, one can show that $\log\langle k\rangle$ is the zeroth-order term in an expansion of $\langle S\rangle$ in the limit of large average degree $\langle k\rangle \gg 1$. Expanding $k \log k$ around $\langle k\rangle$, we find

$$\begin{aligned}\langle S\rangle &= \frac{1}{\langle k\rangle}\langle \langle k\rangle \log\langle k\rangle + (1+\log\langle k\rangle)\,(k-\langle k\rangle) + \frac{(k-\langle k\rangle)^2}{2\langle k\rangle} + O\left(\frac{1}{\langle k\rangle^2}\right)\rangle \\ &= \log\langle k\rangle + \frac{\mathrm{Var}(k)}{2\langle k\rangle^2} + O\left(\frac{1}{\langle k\rangle^3}\right),\end{aligned} \tag{14}$$

where $\mathrm{Var}(k)$ is the variance of k. We therefore find that, in addition to increasing logarithmically with the average degree, the entropy of random walks grows with increasing degree variance. In turn, this result further supports the conclusion that networks with heterogeneous degrees produce random walks with higher entropy. In what follows, we derive analytic results for the entropy of random walks on various canonical network families.

7.2 – k-regular network. We begin by studying k-regular networks, wherein each node i has constant degree $k_i = k$. In this case, we arrive at the simple relation $\langle S\rangle = \log k$, which saturates the lower bound in Eq. (13).[12] This result shows that k-regular networks achieve the lowest possible entropy among networks of a given density.

7.3 – Poisson distributed network. While k-regular networks maintain a lattice-like structure, many real networks display random organization.[35] The simplest model for generating random networks, known as the Erdös-Rényi model,[72] places E edges uniformly at random between pairs of N nodes. In the thermodynamic limit $N \to \infty$, Erdös-Rényi networks follow a Poisson degree distribution $\mathcal{P}(k) = e^{-\langle k\rangle}\langle k\rangle^k/k!$. In this case, the degree variance is given by $\mathrm{Var}(k) = \langle k\rangle$, and applying Eq. (14), we find that

$$\langle S\rangle = \log\langle k\rangle + \frac{1}{2\langle k\rangle} + O\left(\frac{1}{\langle k\rangle^2}\right). \tag{15}$$

Therefore, in the high-$\langle k\rangle$ limit, the entropy of random walks on an Erdös-Rényi network approaches the lower-bound $\langle S\rangle \approx \log\langle k\rangle$. We find that the analytic prediction in Eq. (15) accurately approximates the true entropy of randomly-generated Erdös-Rényi networks across all values of the average degree (Fig. S8a).

To investigate the relationship between the entropy and the heterogeneity of degrees in a

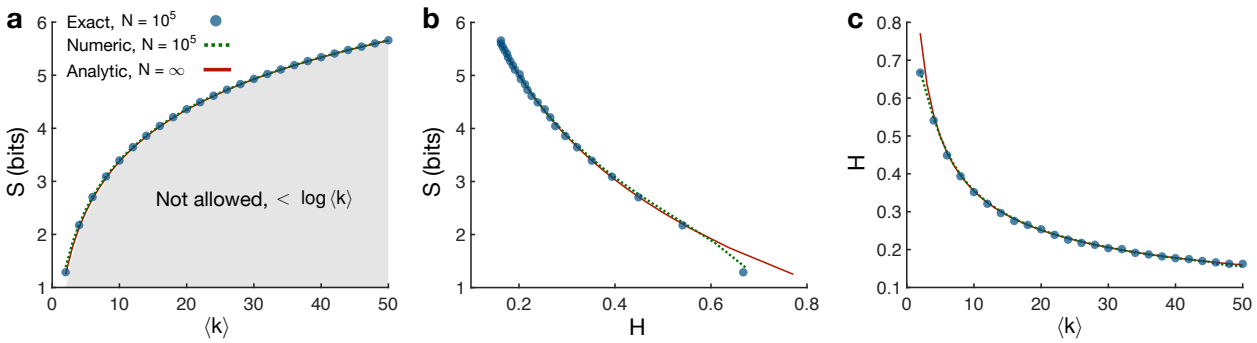

Fig. S8 | Entropy of random walks in Poisson distributed networks.

a, Entropy of random walks as a function of the average degree $\langle k \rangle$ for Poisson distributed networks. Data points are exact calculations using the degree sequences of randomly-generated Erdös-Rényi networks of size $N = 10^4$. Dashed lines are numerical results for $N = 10^4$, calculated using the Poisson degree distribution. Solid lines are analytic results for the thermodynamic limit $N \to \infty$. **b**, Entropy as a function of the degree heterogeneity H for variable $\langle k \rangle$. **c**, Degree heterogeneity as a function of the average degree.

network, we defined the degree heterogeneity to be the relative average difference in degrees,

$$H = \frac{\langle |k_i - k_j| \rangle}{\langle k \rangle} = \frac{1}{\langle k \rangle} \sum_{k_i, k_j} |k_i - k_j| \mathcal{P}(k_i) \mathcal{P}(k_j). \tag{16}$$

H is a well-studied measure of the dispersion of a distribution, with range $[0, 2]$. We note that other often used measures of degree heterogeneity, such as $\langle k^2 \rangle / \langle k \rangle^2$ and $\mathrm{Var}(k)/\langle k \rangle^2$, cannot be used to study the impact of degree heterogeneity on entropy for scale-free networks since $\langle k^2 \rangle$ diverges for $\gamma \leq 3$ in the limit $N \to \infty$. For Poisson distributed networks, one can show that

$$H = 2e^{-2\langle k \rangle} \big(I_0(2\langle k \rangle) + I_1(2\langle k \rangle) \big), \tag{17}$$

where $I_\nu(x)$ is the modified Bessel function of the first kind.[25] For other degree distributions, however, it is generally difficult to derive an analytic form for H. We find that the entropy of random walks on Poisson distributed networks decreases with increasing degree heterogeneity as we vary $\langle k \rangle$ (Fig. S8b), seemingly contradicting our conclusion in the main text that entropy increases with heterogeneity. However, this effect is driven by the monotonic decrease in H with increasing $\langle k \rangle$ in Poisson distributed networks (Fig. S8c). In the following subsections, we show

that entropy does in fact increase with degree heterogeneity for other network models, confirming the results in the main text.

7.4 – Power-law distributed network. Compared to random networks, real networks often contain a number of hub nodes with unusually high degree, leading to a heavy-tailed distribution of node degrees.[35] Often this heavy-tailed distribution is associated with scale-free organization,[21] which is characterized by a power-law degree distribution $\mathcal{P}(k) \sim k^{-\gamma}$, where γ is the scale-free exponent. In the limit $N \to \infty$, we can approximate the averages in Eq. (12) as integrals, and one can show that[3]

$$\langle S \rangle = \frac{1}{\gamma - 2}. \tag{18}$$

We see that the entropy diverges as $\gamma \to 2$, while for $\gamma > 2$ the entropy of scale-free networks is well-defined. We remark that this critical exponent is different from $\gamma = 3$, which is the critical exponent for many other network phenomena driven by the divergence of $\langle k^2 \rangle$.[73,74] Instead, as $\gamma \to 2$, super-hubs emerge that connect to almost all of the nodes in the network, causing the average degree $\langle k \rangle$ to diverge.[35] Each time a random walk arrives at one of these super-hubs, the entropy of the ensuing transition, roughly $-\log \frac{1}{N}$, diverges as $N \to \infty$.

We compare the analytic prediction in Eq. (18) with exact calculations from both power-law distributed networks generated using the configuration model[75] and from numerical calculations of the averages in Eq. (12), finding that the numerical estimates agree well with the exact values (Fig. S9a). Moreover, we find that the entropy increases with degree heterogeneity as we sweep over γ (Fig. S9b), confirming our conclusions in the main text. This increase in entropy is related to the corresponding increase in heterogeneity as $\gamma \to 2$ (Fig. S9c).

7.5 – Static model. In order to test the effects of network density and degree heterogeneity independently, we turn to the static model, which is commonly used to generate scale-free networks of a given density.[24] Beginning with N disconnected nodes, we assign each node i a weight $w_i = i^{-\alpha}$, where $\alpha \in [0, 1)$ is a real number. Then, we randomly select a pair of nodes i and j with probabilities proportional to their weights, and we connect them if they have not already been connected. This process is repeated until $E = \frac{1}{2} N \langle k \rangle$ edges have been added. A number of analytic properties

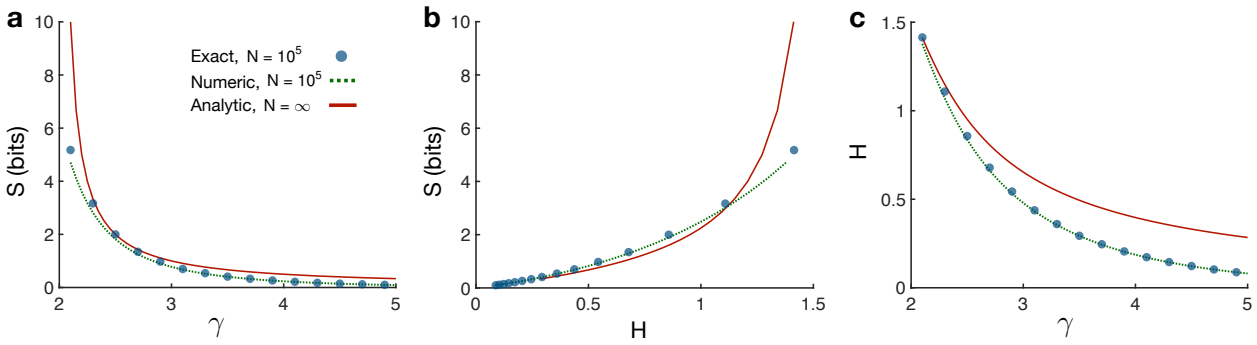

Fig. S9 | Entropy of random walks in power-law distributed networks.

a, Entropy of random walks as a function of the scale-free exponent γ for power-law distributed networks. Data points are exact calculations from networks of size $N = 10^4$ generated using the configuration model.[75] Dashed lines are numerical results for $N = 10^4$, calculated using the power-law degree distribution. Solid lines are analytic results for the thermodynamic limit $N \to \infty$. **b**, Entropy as a function of the degree heterogeneity H for variable γ. **c**, Degree heterogeneity as a function of the scale-free exponent.

have been derived for the static model,[76,77] including the fact that, in the thermodynamic limit, the degree distribution is given by $\mathcal{P}(k) = \frac{1}{\alpha}\left(\frac{\langle k\rangle}{2}(1-\alpha)\right)^{1/\alpha}\frac{\Gamma\left(k-\frac{1}{\alpha},\frac{\langle k\rangle}{2}(1-\alpha)\right)}{\Gamma(k+1)}$, where $\Gamma(\cdot)$ is the gamma function and $\Gamma(\cdot,\cdot)$ is the upper incomplete gamma function. In the large-k limit, one can show that the degree distribution drops off as a power law $\mathcal{P}(k) \sim k^{-\gamma}$, where $\gamma = 1 + \frac{1}{\alpha}$.

We are interested in deriving an analytic form for the entropy. Using a hidden variables method,[76] one can show that the average degree of node i is given by

$$\bar{k}(i) = \langle k\rangle(1-\alpha)\left(\frac{i}{N}\right)^{-\alpha}\left(1 - N^{\alpha-1}\right). \tag{19}$$

Approximating the numerator in Eq. (12) by $\langle k\log k\rangle \approx \frac{1}{N}\int_1^N \bar{k}(i)\log\bar{k}(i)\,di$, and taking the limit $N \to \infty$, we find that the entropy is given by

$$\langle S\rangle = \log\langle k\rangle + \frac{1}{\gamma-2} - \log\frac{\gamma-1}{\gamma-2}. \tag{20}$$

We note that the average degree of a pure power-law network is $\langle k\rangle = \frac{\gamma-1}{\gamma-2}$. Plugging this average degree into Eq. (20), we recover the entropy of power-law distributed networks in Eq. (18), as expected. Interestingly, we notice that, even for finite $\langle k\rangle$, the entropy in the static model diverges as $\gamma \to 2$ in the thermodynamic limit.

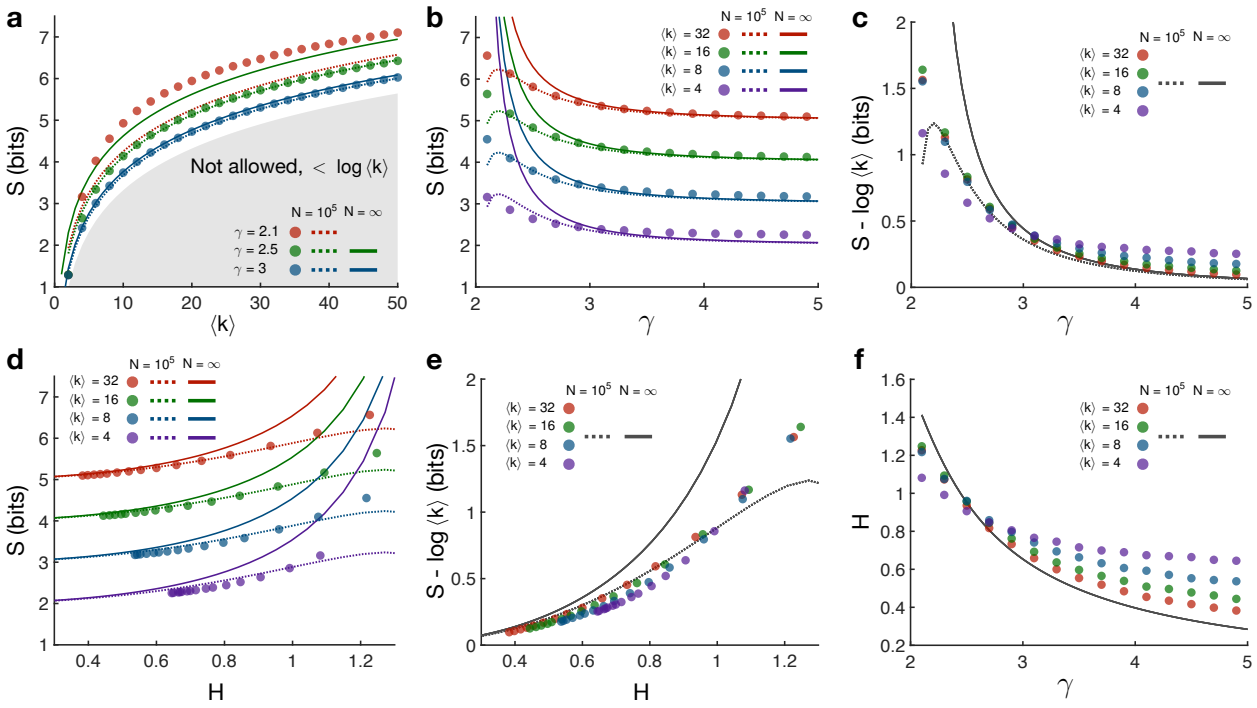

Fig. S10 | Entropy of random walks in static model networks.

a, Entropy of random walks as a function of the average degree $\langle k \rangle$ for various values of the scale-free exponent γ in the static model. Data points are exact calculations using the degree sequences of networks with $N = 10^4$ generated using the static model. Dashed lines are numerical results for $N = 10^4$, calculated using the average degree relationship in Eq. (19). Solid lines are analytic results for the thermodynamic limit $N \to \infty$. **b**, Entropy as a function of γ for various values of $\langle k \rangle$. **c**, The quantity $S - \log\langle k \rangle$ collapses to a single function of γ across various values of $\langle k \rangle$. **d**, Entropy as a function of the degree heterogeneity H for varying γ. **e**, The quantity $S - \log\langle k \rangle$ increases with H for varying γ. **f**, Degree heterogeneity increases as γ decreases toward the critical value $\gamma = 2$.

We find that the entropy increases as $\langle k \rangle$ increases (Fig. S10a) and also as γ decreases (Fig. S10b). The thermodynamic result in Eq. (20) is accurate for $\gamma \geq 3$, while numerical calculations using Eq. (19) and including finite network size yield accurate predictions for $\gamma \geq 2.5$. We note that the only effect of $\langle k \rangle$ on the entropy in Eq. (20) is in the logarithmic lower bound, suggesting that the quantity $S - \log\langle k \rangle$ should depend exclusively on the scale-free exponent γ. Indeed, subtracting $\log\langle k \rangle$ from our entropy calculations, we find that networks of varying density collapse onto a single line (Fig. S10c). This result is made even more clear by considering how the

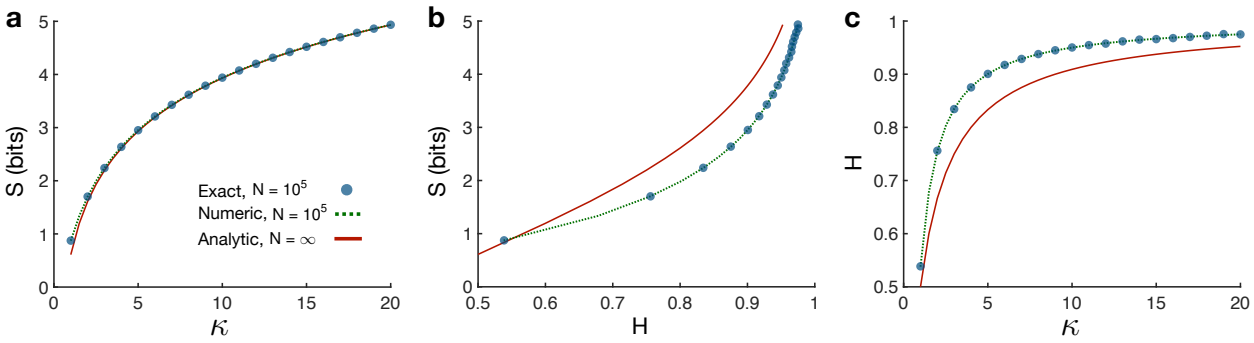

Fig. S11 | Entropy of random walks in exponentially distributed networks.

a, Entropy of random walks as a function of the degree cutoff κ for exponentially distributed networks. Data points are exact calculations from networks of size $N = 10^4$ generated using the configuration model.[75] Dashed lines are numerical results for $N = 10^4$, calculated using the exponential degree distribution. Solid lines are analytic results for the thermodynamic limit $N \to \infty$. **b**, Entropy as a function of the degree heterogeneity for variable κ. **c**, Degree heterogeneity as a function of the exponential cutoff.

quantity $S - \log\langle k\rangle$ varies with degree heterogeneity as we sweep over γ (Fig. S10e). Finally, we note that H increases with decreasing γ (Fig. S10f), thereby explaining the monotonic relationship between entropy and degree heterogeneity in the static model (Fig. S10d).

7.6 – Exponentially distributed network. Many real networks exhibit degree distributions with exponential cutoffs for large values of k.[23,35] In pure exponentially distributed networks, the degree distribution follows the form $\mathcal{P}(k) \sim e^{-k/\kappa}$, where $\kappa \geq 0$ is the degree cutoff. In the thermodynamic limit, approximating the averages in Eq. (12) as integrals, we find that the entropy is given by

$$\langle S\rangle = \log\langle k\rangle + \frac{1-\gamma_{\mathrm{e}}}{\ln 2}, \tag{21}$$

where γ_{e} is Euler's constant. We see in Fig. S11a that this analytic prediction accurately describes the entropy of randomly-generated exponential networks. Moreover, we find that the entropy increases with increasing degree heterogeneity (Fig. S11b) and that the heterogeneity increases with the degree cutoff κ (Fig. S11c).

8 KL divergence between random walks and human expectations

The results of the previous section demonstrate that, generally, the entropy of random walks is larger for networks with heterogeneous degrees, a feature that has been found in many real networks.[21–23,78] But what are the structural features that allow a network to maintain a low divergence from human expectations? Here, we answer this question by studying the KL divergence $D_{\text{KL}}(P||\hat{P})$ between a network's transition structure P and the expectations of an observer $\hat{P}$.

8.1 – Upper bound. For expectations $\hat{P}$ of the form in Eq. (9), the KL divergence is given by

$$\begin{aligned} D_{\text{KL}}(P||\hat{P}) &= -\sum_i \pi_i \sum_j P_{ij} \log \frac{\hat{P}_{ij}}{P_{ij}} \\ &= -\sum_i \pi_i \sum_j P_{ij} \log \left(C \sum_{t=1}^{\infty} g(t) \frac{(P^t)_{ij}}{P_{ij}} \right), \end{aligned} \tag{22}$$

where $(P^t)_{ij}/P_{ij}$ is the relative probability of transitioning from node i to node j in t steps versus one step. Keeping only the first term inside the logarithm, we arrive at an upper bound for the KL divergence,

$$D_{\text{KL}}(P||\hat{P}) \leq -\sum_i \pi_i \sum_j P_{ij} \log \left(C g(1) \right) = -\log \left(C g(1) \right). \tag{23}$$

Eq. (23) allows us to make a number of simple predictions for the KL divergence. For example, if the expectations are defined by $g(t) = \eta^{t-1}$, as presented in the main text, then $C = 1 - \eta$ and so $D_{\text{KL}} \leq -\log(1-\eta)$. In this case, we see that the KL divergence tends to zero as $\eta \to 0$ and that the upper bound diverges as $\eta \to 1$. In contrast, if $g(t) = t^{-\alpha}$ then $C = \zeta(\alpha)^{-1}$, where $\zeta(\cdot)$ is the Riemann zeta function, and we have $D_{\text{KL}} \leq \log \zeta(\alpha)$. As a final example, if $g(t) = 1/t!$ then $C = (e-1)^{-1}$, and so $D_{\text{KL}} \leq \log(e-1)$.

8.2 – Relationship to clustering. While Eq. (23) provides a simple relationship between the KL divergence and parameters in the model for $\hat{P}$, we are ultimately interested in understanding the effects of network structure. To gain an intuition for the role of topology, it helps to focus on a particular model for the expectations. For example, considering $g(t) = \eta^{t-1}$, in the low-η limit the

KL divergence takes the form

$$\begin{aligned} D_{\rm KL}(P||\hat{P}) &= -\log(1-\eta) - \sum_i \pi_i \sum_j P_{ij} \log\left(1 + \eta \frac{(P^2)_{ij}}{P_{ij}} + O(\eta^2)\right) \\ &= -\log(1-\eta) - \frac{\eta}{\ln 2} \sum_i \pi_i \sum_j P_{ij} \frac{(P^2)_{ij}}{P_{ij}} + O(\eta^2). \end{aligned} \tag{24}$$

We note that, when calculating information measures such as entropy or KL divergence, one only considers terms with non-zero probability, such that, for each node i, the sum on j in Eq. (24) implicitly runs over all nodes for which $P_{ij} = \frac{1}{k_i} G_{ij}$ is non-zero. Therefore, for undirected networks, recalling that $\pi_i = \frac{k_i}{2E}$, we have

$$D_{\rm KL}(P||\hat{P}) = -\log(1-\eta) - \frac{\eta}{2E \ln 2} \sum_i k_i \sum_j G_{ij} \sum_\ell \left(\frac{1}{k_i} G_{i\ell}\right)\left(\frac{1}{k_\ell} G_{\ell j}\right) + O(\eta^2). \tag{25}$$

Switching the i and ℓ indices and canceling terms, we arrive at the concise approximation

$$D_{\rm KL}(P||\hat{P}) = -\log(1-\eta) - \frac{\eta}{2E \ln 2} \sum_i \frac{1}{k_i} \triangle_i + O(\eta^2), \tag{26}$$

where $\triangle_i = (G^3)_{ii}$ is the number of (possibly weighted) triangles involving node i. We therefore find that the KL divergence is lower for networks with a lager number of triangles or, equivalently, a higher clustering coefficient. In the following subsections, we investigate the relationship between KL divergence and clustering in Erdös-Rényi and stochastic block networks.

8.3 – Erdös-Rényi network. We wish to derive an analytic approximation for the KL divergence of an Erdös-Rényi network. Considering human expectations defined by $g(t) = \eta^{t-1}$, for undirected networks Eq. (22) becomes

$$\begin{aligned} D_{\rm KL}(P||\hat{P}) &= -\sum_i \frac{k_i}{2E} \sum_j \frac{1}{k_i} G_{ij} \log\left((1-\eta) \sum_{t=1}^{\infty} \eta^{t-1} \frac{(P^t)_{ij}}{P_{ij}}\right) \\ &= -\log(1-\eta) - \frac{1}{2E} \sum_{ij} G_{ij} \log\left(\sum_{t=1}^{\infty} \eta^{t-1} \frac{(P^t)_{ij}}{P_{ij}}\right). \end{aligned} \tag{27}$$

We note that the second term above is an average of the logarithm over the edges in the network. Approximating this average of logarithms by a logarithm of the average, we have

$$D_{\rm KL}(P||\hat{P}) \approx -\log(1-\eta) - \log\left[\frac{1}{2E} \sum_{ij} k_i G_{ij} \sum_{t=1}^{\infty} \eta^{t-1} (P^t)_{ij}\right]. \tag{28}$$

For unweighted networks, we recognize that $\sum_j G_{ij}(P^t)_{ij}$ is the probability of transitioning from node i to one of i's neighbors in t steps. For $t = 1$ this probability is one. For $t > 1$, we consider two cases: (i) dense networks with high $\langle k \rangle$, and (ii) sparse networks with low $\langle k \rangle$.

For dense networks, we approximate the probability of transitioning from node i to one of node i's neighbors in $t > 1$ steps as k_i/N, the probability of randomly selecting one of the k_i neighbors from all N nodes. Plugging this approximation for $\sum_j G_{ij}(P^t)_{ij}$ into Eq. (28), we have

$$\begin{aligned} D_{\text{KL}}(P||\hat{P}) &\approx -\log(1-\eta) - \log\left[\frac{1}{2E}\sum_i k_i\left(1 + \sum_{t=2}^{\infty}\eta^{t-1}\frac{k_i}{N}\right)\right] \\ &= -\log(1-\eta) - \log\left[1 + \frac{1}{2EN}\frac{\eta}{1-\eta}\sum_i k_i^2\right]. \end{aligned} \tag{29}$$

We have now reduced the KL divergence to a function of the degree sequence $\boldsymbol{k}$. For large Erdös-Rényi networks, the node degrees follow a Poisson distribution, and, for large $\langle k \rangle$, we have $\langle k^2 \rangle \approx \langle k \rangle^2$. Thus, the average KL divergence for a dense Erdös-Rényi network can be approximated by

$$\begin{aligned} \langle D_{\text{KL}} \rangle &\approx -\log(1-\eta) - \langle \log\left[1 + \frac{1}{2E}\frac{\eta}{1-\eta}k^2\right] \rangle \\ &\approx -\log(1-\eta) - \log\left[1 + \frac{1}{2E}\frac{\eta}{1-\eta}\langle k^2 \rangle\right] \\ &\approx -\log(1-\eta) - \log\left[1 + \frac{1}{2E}\frac{\eta}{1-\eta}\langle k \rangle^2\right] \\ &= -\log\left[1 - \eta\left(1 - \frac{\langle k \rangle}{N}\right)\right], \end{aligned} \tag{30}$$

where the averages are taken over the degree distribution $\mathcal{P}(k)$. We find that this approximation accurately predicts the KL divergence of Erdös-Rényi networks as a function of the integration parameter η (Fig. S12a). We also see that in the thermodynamic limit $N \to \infty$, D_{KL} approaches the upper bound $-\log(1-\eta)$.

For sparse Erdös-Rényi networks, the number of loops is small and thus the network is locally treelike.[79] In a tree, the probability $\sum_j G_{ij}(P^t)_{ij}$ of transitioning from a given node i to one of node i's neighbors is zero if t is even. For t odd, setting node i to be the root of the tree, if we assume all nodes have the same degree $\langle k \rangle$, then the probability of moving down the tree

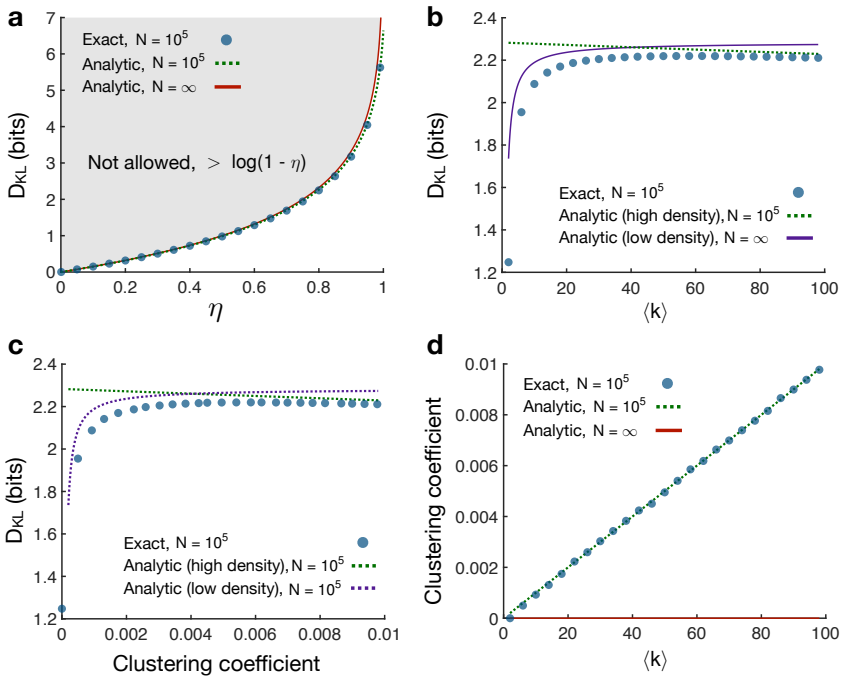

Fig. S12 | KL divergence from human expectations in Erdös-Rényi networks.

a, KL divergence between random walks and human expectations as a function of the inaccuracy parameter η for Erdös-Rényi networks. Data points are exact calculations for networks of size $N = 10^4$ with average degree $\langle k \rangle = 100$. Dashed line is the analytic prediction using Eq. (30) with $N = 10^4$. Solid line is the analytic result for the thermodynamic limit $N \to \infty$. **b**, KL divergence as a function of the average degree $\langle k \rangle$ for η equal to the value 0.80 measured in the serial response experiments. Dashed line represents the high-density analytic approximation in Eq. (30) with $N = 10^4$, while the solid line is the low-density approximation in Eq. (32). **c**, KL divergence as a function of the average clustering coefficient for variable $\langle k \rangle$. **d**, Average clustering coefficient as a function of $\langle k \rangle$. In the thermodynamic limit the clustering tends toward zero for all values of $\langle k \rangle$ (solid line).

on any given step is $1 - 1/\langle k \rangle$ and the probability of moving up the tree is $1/\langle k \rangle$. Approximating $1 - 1/\langle k \rangle \approx 1$, then the probability of moving down the tree $(t + 1)/2$ steps and back up the tree

$(t-1)/2$ steps is roughly $1/\langle k\rangle^{\frac{t-1}{2}}$. Plugging this expression into Eq. (28), we have

$$\begin{aligned} D_{\mathrm{KL}}(P||\hat{P}) &\approx -\log(1-\eta) - \log\left[\frac{1}{2E}\sum_i k_i \sum_{t\ \mathrm{odd}} \eta^{t-1}\langle k\rangle^{-\frac{t-1}{2}}\right] \\ &= -\log(1-\eta) - \log\left[\frac{1}{2E}\sum_i k_i \sum_{t=0}^{\infty} \eta^{2t}\langle k\rangle^{-t}\right] \\ &= -\log(1-\eta) - \log\left[\frac{1}{2E}\frac{\langle k\rangle}{\langle k\rangle-\eta^2}\sum_i k_i\right]. \end{aligned} \tag{31}$$

Averaging over the Poisson degree distribution, we have

$$\begin{aligned} \langle D_{\mathrm{KL}}\rangle &\approx -\log(1-\eta) - \left\langle \log\left[\frac{N}{2E}\frac{\langle k\rangle}{\langle k\rangle-\eta^2}k\right]\right\rangle \\ &\approx -\log(1-\eta) - \log\left[\frac{\langle k\rangle}{\langle k\rangle-\eta^2}\right]. \end{aligned} \tag{32}$$

We find that the above approximation provides a decent estimate of the KL divergence for low $\langle k\rangle$, while the high-density approximation in Eq. (30) accurately predicts the KL divergence for $\langle k\rangle > 50$ (Fig. S12b).

In addition to the dependence of D_{KL} on η and $\langle k\rangle$, we are also interested in the effect of clustering. The clustering coefficient of a given node i is the number of triangles $\triangle_i$ involving node i divided by the number of possible triangles $\binom{k_i}{2} = k_i(k_i-1)/2$. For Erdös-Rényi networks, averaging over all nodes i, the clustering coefficient is approximately $\langle k\rangle/N$. We find that, for small $\langle k\rangle$, the KL divergence increases with increasing clustering, while, for large $\langle k\rangle$, the KL divergence decreases (Fig. S12c). Given that the clustering is directly proportional to $\langle k\rangle$ in Erdös-Rényi networks (Fig. S12d), the effects of clustering on D_{KL} are driven by the density of the network. To disambiguate the effects of clustering and density, in the following subsection, we study a stochastic block model in which these properties can be varied independently.

8.4 – Stochastic block network. In order to test the effects of clustering on the KL divergence without the confounding impact of edge density, we consider the stochastic block model.[80] Specifically, the N nodes are divided into N/n communities of n nodes each. Then, a prescribed fraction f of the $E = \langle k\rangle N/2$ edges are placed between pairs of nodes within the same community, and the remaining fraction $1-f$ of edges are placed between nodes in different communities.

We wish to understand the dependence of the KL divergence on the fraction f of within-community edges. Beginning with Eq. (28), we once again consider the probability $\sum_j G_{ij}(P^t)_{ij}$ of transitioning from node i to one of node i's neighbors in t steps. As before, for $t = 1$ this probability is one. For $t > 1$, we approximate

$$\sum_j G_{ij}(P^t)_{ij} \approx p^{\text{in}}(t)\frac{k_i^{\text{in}}}{n-1} + p^{\text{out}}(t)\frac{k_i^{\text{out}}}{N-n}, \tag{33}$$

where $p^{\text{in}}(t)$ is the probability of ending up in the same community as node i after t steps, $p^{\text{out}}(t)$ is the probability of ending up in a different community from node i after t steps, $k_i^{\text{in}} \approx fk_i$ is the number of edges connecting node i to nodes within the same community, and $k_i^{\text{out}} \approx (1-f)k_i$ is the number of edges connecting node i with nodes in different communities. We model the transitions in and out of node i's community as a two-state Markov process with probability matrix

$$A = \begin{pmatrix} P(\text{in} \mid \text{in}) & P(\text{in} \mid \text{out}) \\ P(\text{out} \mid \text{in}) & P(\text{out} \mid \text{out}) \end{pmatrix} = \begin{pmatrix} f & 1-f \\ \frac{n}{N-n}(1-f) & f + \frac{N-2n}{N-n}(1-f) \end{pmatrix}. \tag{34}$$

Using this representation, one can show that

$$\begin{aligned} p^{\text{in}}(t) = (A^t)_{11} &\approx \frac{1}{N}\left(n + (N-n)f^t\right), \\ \text{and} \quad p^{\text{out}}(t) = (A^t)_{12} &\approx \frac{N-n}{N}(1-f^t), \end{aligned} \tag{35}$$

where the approximations follow from the assumption that $\left(\frac{fN-n}{N-n}\right)^t \approx f^t$. Plugging Eq. (35) into Eq. (33), we have

$$\begin{aligned} \sum_j G_{ij}(P^t)_{ij} &\approx \frac{fk_i}{N}\left(1 + f^t\left(\frac{N}{n} - 1\right)\right) + \frac{(1-f)k_i}{N}\left(1 - f^t\right) \\ &= \frac{k_i}{N}\left(1 + f^t\left(\frac{N}{n}f - 1\right)\right) \\ &\approx \frac{k_i}{N}\left(1 + \frac{N}{n}f^t\right), \end{aligned} \tag{36}$$

where the final approximation follows from the assumption that $\frac{N}{n}f \gg 1$. We substitute this result

into Eq. (28), finding that

$$\begin{aligned} D_{\mathrm{KL}}(P||\hat{P}) &\approx -\log(1-\eta) - \log\left[\frac{1}{2E}\sum_i k_i\left(1 + k_i\sum_{t=2}^{\infty}\eta^{t-1}\left(\frac{1}{N}+\frac{f^{t+1}}{n}\right)\right)\right] \\ &= -\log(1-\eta) - \log\left[1 + \frac{1}{2E}\sum_i k_i^2\sum_{t=2}^{\infty}\eta^{t-1}\left(\frac{1}{N}+\frac{f^{t+1}}{n}\right)\right] \\ &= -\log(1-\eta) - \log\left[1 + \frac{1}{2E}\left(\frac{1}{N}\frac{\eta}{1-\eta} + \frac{1}{n}\frac{\eta f^3}{1-\eta f}\right)\sum_i k_i^2\right] \\ &= -\log\left[1 - \eta + \frac{\eta}{2E}\left(\frac{1}{N} + \frac{1}{n}\frac{(1-\eta)f^3}{1-\eta f}\right)\sum_i k_i^2\right]. \end{aligned} \tag{37}$$

For stochastic block models in the thermodynamic limit $N \to \infty$, the degree distribution is Poisson, and for large $\langle k\rangle$ we have $\langle k^2\rangle \approx \langle k\rangle^2$. Averaging over the Poisson degree distribution, the average KL divergence can be approximated by

$$\begin{aligned} \langle D_{\mathrm{KL}}\rangle &\approx -\left\langle \log\left[1 - \eta + \frac{\eta}{2E}\left(\frac{1}{N} + \frac{1}{n}\frac{(1-\eta)f^3}{1-\eta f}\right)\sum_i k_i^2\right]\right\rangle \\ &\approx -\log\left[1 - \eta + \frac{\eta N}{2E}\left(\frac{1}{N} + \frac{1}{n}\frac{(1-\eta)f^3}{1-\eta f}\right)\langle k^2\rangle\right] \\ &\approx -\log\left[1 - \eta\left(1 - \frac{\langle k\rangle}{N} - \frac{\langle k\rangle}{n}\frac{(1-\eta)f^3}{1-\eta f}\right)\right]. \end{aligned} \tag{38}$$

We remark that the first three terms inside the logarithm in Eq. (38) are identical to the Erdös-Rényi result in Eq. (30), and thus the final term can be regarded as a correction resulting from the modular structure of the stochastic block model. Interestingly, this third term does not vanish in the thermodynamic limit $N \to \infty$; however, it does vanish in the limit $f \to 0$, as the network loses its block structure. We find that the analytic prediction in Eq. (38) is accurate across all values of η and all fractions f (Fig. S13a,b). Furthermore, we find that the KL divergence decreases monotonically with increasing f for fixed average degree $\langle k\rangle$ (Fig. S13a,b).

In order to predict the effect of clustering, it is helpful to have an analytic approximation for the average clustering coefficient in a stochastic block network. We recall that the clustering coefficient for a node i is given by $2\triangle_i/(k_i(k_i-1))$, where $\triangle_i$ is the number of triangles involving node i. For a stochastic block network, we define the probability of an edge existing between two

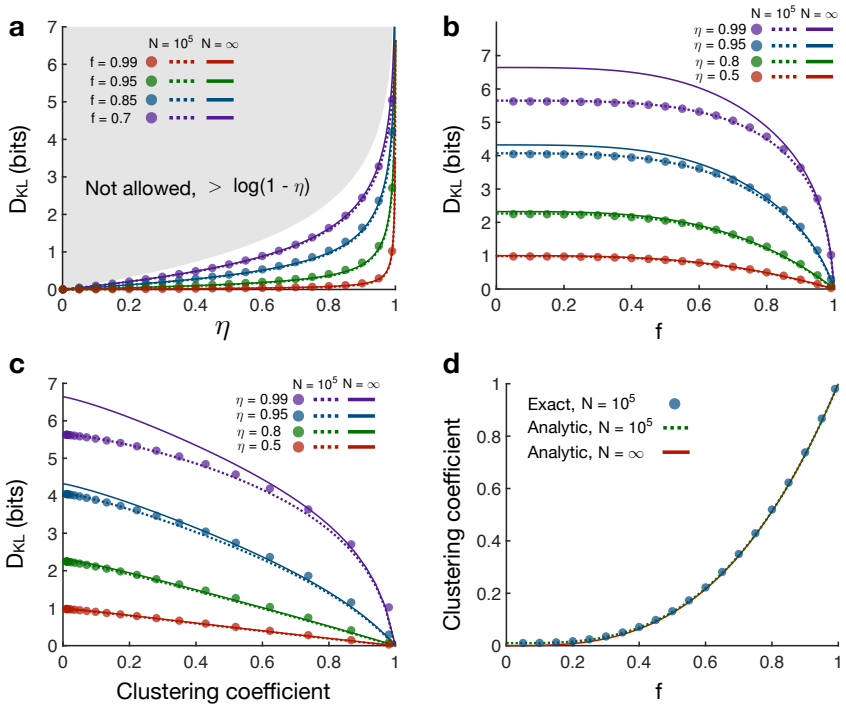

Fig. S13 | KL divergence from human expectations in stochastic block networks.

a, KL divergence as a function of the integration parameter η for stochastic block networks with average degree $\langle k \rangle = 100$ and communities of size $n = 100$. Data points are exact calculations for networks of size $N = 10^4$. Dashed lines are analytic predictions using Eq. (38) with $N = 10^4$. Solid lines are analytic results for the thermodynamic limit $N \to \infty$. **b**, KL divergence as a function of the fraction of within-community edges f for different values of η. **c**, KL divergence as a function of the average clustering coefficient for variable f and different values of η. **d**, Average clustering coefficient as a function of f. Dashed line is the analytic prediction in Eq. (41) with $N = 10^4$. Solid line is the analytic result in the limit $N \to \infty$.

nodes in the same community as $p^{\text{in}} = f\langle k \rangle / n$ and the probability of an edge between two nodes in different communities as $p^{\text{out}} = (1-f)\langle k \rangle / (N-n)$. We then arrive at the following approximation,

$$\begin{aligned} \langle \triangle_i \rangle &= \frac{k_i^{\text{in}}(k_i^{\text{in}}-1)}{2} p^{\text{in}} + k_i^{\text{in}} k_i^{\text{out}} p^{\text{out}} + \frac{k_i^{\text{out}}(k_i^{\text{out}}-1)}{2} \left[\frac{n-1}{N-n-1} p^{\text{in}} + \left(\frac{N-2n}{N-n-1} \right) p^{\text{out}} \right] \\ &\approx \frac{p^{\text{in}}}{2} (k_i^{\text{in}})^2 + p^{\text{out}} k_i^{\text{out}} \left(k_i^{\text{in}} + \frac{k_i^{\text{out}}}{2} \right), \end{aligned} \tag{39}$$

where the approximation follows from the assumptions that $N \gg n$ and $k_i^{\text{in}}, k_i^{\text{out}} \gg 1$. Plugging in

for p^{in}, p^{out}, $k_i^{\text{in}} = fk_i$, and $k_i^{\text{out}} = (1-f)k_i$, we have

$$\langle \triangle_i \rangle \approx \frac{\langle k \rangle k_i^2}{2} \left(\frac{f^3}{n} + \frac{(1+f)(1-f)^2}{N-n} \right). \tag{40}$$

Thus the average clustering coefficient is given by

$$\frac{1}{N} \sum_i \frac{2\langle \triangle_i \rangle}{k_i(k_i-1)} \approx \langle k \rangle \left(\frac{f^3}{n} + \frac{(1+f)(1-f)^2}{N-n} \right), \tag{41}$$

where the approximation follows from the assumption that $k_i \gg 1$. We see that this analytic result accurately predicts the increase in the average clustering coefficient with increasing modularity f (Fig. S13d). More importantly, we find that the KL divergence decreases with increasing clustering for fixed η and $\langle k \rangle$ (Fig. S13c). This final result indicates that increased modularity helps human observers maintain accurate representations, thereby reducing their inefficiency when processing information.

9 Hierarchically modular networks

The combination of high entropy and low KL divergence exhibited by real networks is driven by heterogeneous degrees and modular structure. Interestingly, degree heterogeneity and modularity are ubiquitous in natural and human-made systems,[2,21,22,26–28,78] and together they define hierarchically modular organization.[29] In order to simultaneously study entropy and KL divergence, it is helpful to have a model for generating networks with variable heterogeneity and modularity. One of the earliest models of hierarchical systems was developed to understand metabolic networks.[29,81] Yet this model is deterministic, generating fractal networks in which it is difficult to tune the heterogeneity or modularity. Another common model is the nested stochastic block model,[82,83] wherein small modules are nested inside larger modules. However, this model does not include heterogeneous degrees (a heavy-tailed degree distribution). Perhaps the closest model to what we require was recently developed to study the emergence of complex dynamics in the brain.[84] In this model, the nested stochastic block model is combined with a preferential attachment rule to generate a rich club of hub nodes.

Here we propose a model that directly combines the static model[24,76,77] and the stochastic

block model.[80] Beginning with N disconnected nodes, we first assign each node i a weight $w_i = i^{-\alpha}$, where $\alpha \in [0, 1]$ is related to the scale-free exponent by $\gamma = 1 + \frac{1}{\alpha}$. We also assign each node i to a community. Then, we randomly select pairs of nodes i and j within the same community with probabilities proportional to their weights, and we connect them if they have not already been connected. This process is repeated until $fE = \frac{1}{2}f\langle k\rangle N$ edges have been added within communities. We then repeat this process again until $(1-f)E = \frac{1}{2}(1-f)\langle k\rangle N$ edges have been added between communities. The resulting network has a degree distribution that drops off as a power law $\mathcal{P}(k) \sim k^{-\gamma}$ and also has the same community structure as a stochastic block model.

Sweeping over the two parameters γ and f, while fixing the average degree $\langle k\rangle = 100$ and community size $n = 100$, we see that our hierarchically modular model exhibits a variety of entropies (Fig. S14a) and KL divergences (Fig. S14b). Additionally, we verify that the model can attain a wide range of degree heterogeneities (Fig. S14c) and clustering coefficients (Fig. S14d). Notably, the variation in the degree heterogeneity and clustering coefficient with γ and f appears almost identical to the variation in the entropy and KL divergence, respectively, once again indicating that entropy is primarily driven by heterogeneity and KL divergence is primarily driven by clustering or modularity.

Given our investigation of the information properties of different network models, it is ultimately important to compare against real communication networks. For each network listed in Table S6, we generate series of scale-free networks with various exponents γ, stochastic block networks with various within-community fractions f, and hierarchically modular networks with various exponents γ (for fixed f) and various f (for fixed γ). Each model network maintains the same number of nodes N and edges E as the corresponding real network. For the stochastic block and hierarchically modular networks, we choose community sizes that are roughly the square root of the network size $n \approx \sqrt{N}$ for the purpose of remaining consistent with our model-based analysis (wherein $N = 10^4$ and $n = \sqrt{10^4} = 100$). Comparing each real and model network with completely randomized versions of the same networks (Fig. S15), we find that: (i) scale-free networks cannot attain the low KL divergence displayed by real networks and (ii) stochastic block

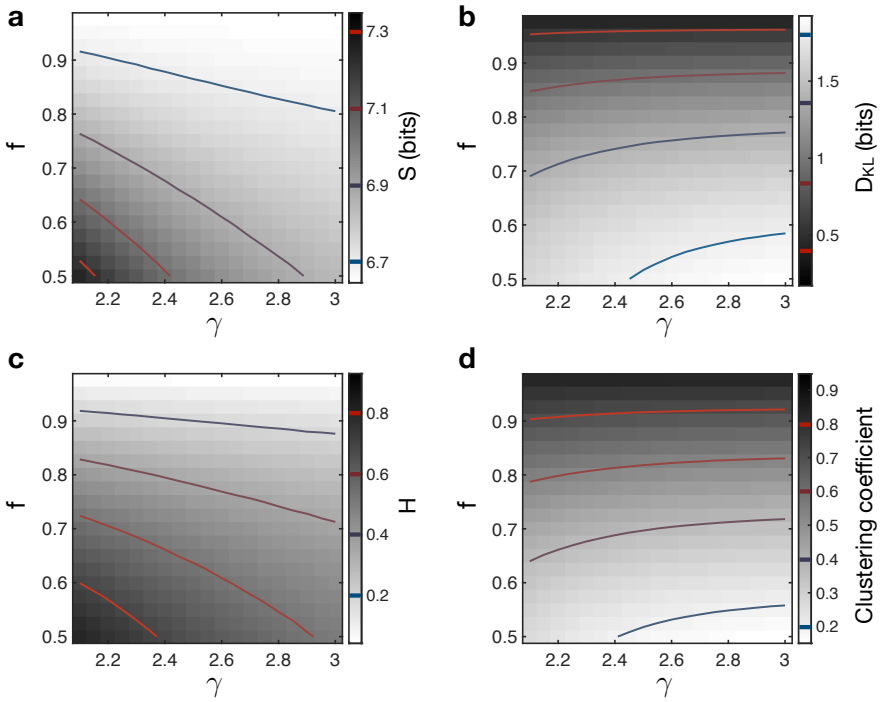

Fig. S14 | Information and structural properties of hierarchically modular networks.

a, Entropy as a function of the scale-free exponent γ and the fraction of within-community edges f for hierarchically modular networks with average degree $\langle k \rangle = 100$ and communities of size $n = 100$. Each point is an exact calculation for a network of size $N = 10^4$. **b**, KL divergence as a function of γ and f in the same networks with η fixed to the average value 0.80 from our experiments. **c**, Degree heterogeneity H varies as a function of γ and f in a similar fashion to the entropy (**a**). **d**, Average clustering coefficient varies as a function of γ and f much like the KL divergence (**b**).

networks cannot attain the high entropy displayed by real networks, but (iii) hierarchically modular networks can achieve both with a parameter combination of $\gamma \approx 2.2$ and $f \approx 0.72$. Thus, we confirm that both heterogeneous degrees and modular structure are required (that is, hierarchical organization is required) to match the information properties of real networks.

10 Network datasets

The real-world networks analyzed in the main text are listed and briefly described in Table S6. While the semantic, web, citation, and social networks are gathered from online network reposito-

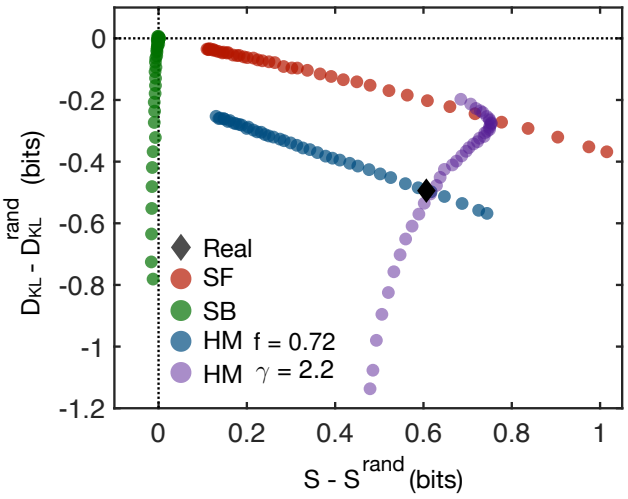

Fig. S15 | Comparing the information properties of real and model networks.

Entropies and KL divergences of real and model networks compared to fully randomized versions. For each model network in Table 1, we generate SF networks with variable γ (red), SB networks with communities of size $n \approx \sqrt{N}$ and variable f (green), and HM networks with $n \approx \sqrt{N}$ and variable γ (fixed $f = 0.72$; blue) or variable f (fixed $\gamma = 2.2$; purple), all with the same number of nodes N and edges E as the real network. Each real and model network is then compared with 100 randomized versions; data points are first averaged over the 100 randomized networks and then averaged over the set of real networks in Table 1. HM networks with $\gamma = 2.2$ and $f = 0.72$ match the average entropy and KL divergence of real networks.

ries, the language and music networks are novel. For the language networks, we developed code to (i) remove punctuation and white space, (ii) filter words by their part of speech, and (iii) record the transitions between the filtered words. Here we focus on networks of transitions between nouns, noting that the same methods could be used to record transitions between other parts of speech. The raw text was gathered from Project Gutenberg (`gutenberg.org/wiki/Main_Page`).

For the music networks, we read in audio files in MIDI format using the `readmidi` function in MATLAB (R2018a). For each song, we split the notes by their channel, which represents the different instruments. For each channel, we created a network of note transitions. We then create a transition network representing the entire song by aggregating the transitions between notes across the different channels. The MIDI files were gathered from `midiworld.com` and from

kunstderfuge.com. Our code and data are available upon request from the corresponding author.

Type	Name	N	E	Description
Language	Shakespeare[85,*]	11,234	97,892	Noun transitions in Shakespeare's work.
	Homer[86,*]	3,556	23,608	Same as above (Homer's Iliad).
	Plato[87,*]	2,271	9,796	Same as above (Plato's Republic).
	Jane Austen[88,*]	1,994	12,120	Same as above (Pride and Prejudice).
	William Blake[89,*]	370	781	Same as above (Songs of Innocence...).
	Miguel de Cervantes[90,*]	6,090	43,682	Same as above (Don Quixote).
	Walt Whitman[91,*]	4,791	16,526	Same as above (Leaves of Grass).
Semantic	Bible[92]	1,707	9,059	Pronoun co-occurrences in Bible verses.
	Les Miserables[92]	77	254	Character co-occurrences.
	Edinburgh Thesaurus[93,94,*]	7,754	226,518	Word similarities in human experiments.
	Roget Thesaurus[94,95,*]	904	3,447	Linked semantic categories.
	Glossary terms[94]	60	114	Words used in definitions of other words.
	FOLDOC[94,96,*]	13,274	90,736	Same as above (computing terms).
	ODLIS[94,97,*]	1,802	12,378	Same as above (information science terms).
Web	Google internal[92,98,*]	12,354	142,296	Hyperlinks between Google's own cites.
	Education[99,100]	2,622	6,065	Hyperlinks between education webpages.
	EPA[100,101]	2,232	6,876	Pages linking to www.epa.gov.
	Indochina[100,102]	9,638	45,886	Hyperlinks between pages in Indochina.
	2004 Election blogs[92,103,*]	793	13,484	Hyperlinks between blogs on US politics.
	Spam[100,104]	3,796	36,404	Hyperlinks between spam pages.
	WebBase[100,102]	6,843	16,374	Hyperlinks gathered by web crawler.
Citations	arXiv Hep-Ph[92,105,*]	12,711	139,500	Citations in Hep-Ph section of the arXiv.
	arXiv Hep-Th[92,105,*]	7,464	115,932	Citations in Hep-Th section of the arXiv.
	Cora[92,106,*]	3,991	16,621	Citation network between scientific papers.
	DBLP[92,107,*]	240	858	Citation network between scientific papers.
Social	Facebook[92,108]	13,130	75,562	Subset of the Facebook network.
	arXiv Astr-Ph[92,105]	17,903	196,972	Coauthorships in Astr-Ph section of arXiv.
	Adolescent health[92,109,*]	2,155	8,970	Friendships between students.
	Highschool[92,110,*]	67	267	Friendships between highschool students.
	Jazz[92,111]	198	2,742	Collaborations between jazz musicians.
	Karate club[92,112]	34	78	Interactions between karate club members.
Music	Thriller – Michael Jackson[113,*]	67	446	Network of note transitions.
	Hard Day's Night – Beatles[114,*]	41	212	Same as above.
	Bohemian Rhapsody – Queen[115,*]	71	961	Same as above.
	Africa – Toto[116,*]	39	163	Same as above.
	Sonata No 11 – Mozart[117,*]	55	354	Same as above.
	Sonata No 23 – Beethoven[118,*]	69	900	Same as above.
	Nocturne Op 9-2 – Chopin[119,*]	59	303	Same as above.
	Clavier Fugue 13 – Bach[120,*]	40	143	Same as above.
	Ballade Op 10-1 – Brahms[121,*]	69	670	Same as above.

Table S6 | Real networks analyzed in the main text. For each network we list its type; name, reference, and whether it has a directed version (denoted by *); number of nodes N; number of edges E; and a brief description.

References

1. Shannon, C. E. A mathematical theory of communication. *Bell Syst. Tech. J.* **27**, 379–423 (1948).

2. Rosvall, M. & Bergstrom, C. T. Maps of random walks on complex networks reveal community structure. *Proc. Natl. Acad. Sci. U.S.A.* **105**, 1118–1123 (2008).

3. Gómez-Gardeñes, J. & Latora, V. Entropy rate of diffusion processes on complex networks. *Phys. Rev. E* **78**, 065102 (2008).

4. Liben-Nowell, D. & Kleinberg, J. Tracing information flow on a global scale using internet chain-letter data. *Proc. Natl. Acad. Sci. U.S.A.* **105**, 4633–4638 (2008).

5. Rosvall, M., Trusina, A., Minnhagen, P. & Sneppen, K. Networks and cities: An information perspective. *Phys. Rev. Lett.* **94**, 028701 (2005).

6. Bar-Hillel, Y. & Carnap, R. Semantic information. *Br. J. Philos. Sci.* **4**, 147–157 (1953).

7. Cohen, J. E. Information theory and music. *Behav. Sci.* **7**, 137–163 (1962).

8. Dretske, F. I. *Knowledge and the Flow of Information* (1981).

9. Hilbert, M. Toward a synthesis of cognitive biases: How noisy information processing can bias human decision making. *Psychol. Bull.* **138**, 211 (2012).

10. Laming, D. R. J. *Information theory of choice-reaction times.* (Academic Press, 1968).

11. Koechlin, E. & Hyafil, A. Anterior prefrontal function and the limits of human decision-making. *Science* **318**, 594–598 (2007).

12. Cover, T. M. & Thomas, J. A. *Elements of information theory* (John Wiley & Sons, 2012).

13. Saffran, J. R., Aslin, R. N. & Newport, E. L. Statistical learning by 8-month-old infants. *Science* **274**, 1926–1928 (1996).

14. Dehaene, S., Meyniel, F., Wacongne, C., Wang, L. & Pallier, C. The neural representation of sequences: From transition probabilities to algebraic patterns and linguistic trees. *Neuron* **88**, 2–19 (2015).

15. Schapiro, A. C., Rogers, T. T., Cordova, N. I., Turk-Browne, N. B. & Botvinick, M. M. Neural representations of events arise from temporal community structure. *Nat. Neurosci.* **16**, 486–492 (2013).

16. Kahn, A. E., Karuza, E. A., Vettel, J. M. & Bassett, D. S. Network constraints on learnability of probabilistic motor sequences. *Nat. Hum. Behav.* **2**, 936 (2018).

17. Lynn, C. W., Kahn, A. E. & Bassett, D. S. Structure from noise: Mental errors yield abstract representations of events. *Submitted, <arxiv.org/abs/1805.12491 >* (2018).

18. Momennejad, I. *et al.* The successor representation in human reinforcement learning. *Nat. Hum. Behav.* **1**, 680 (2017).

19. Gershman, S. J., Moore, C. D., Todd, M. T., Norman, K. A. & Sederberg, P. B. The successor representation and temporal context. *Neural Comput.* **24**, 1553–1568 (2012).

20. Maslov, S. & Sneppen, K. Specificity and stability in topology of protein networks. *Science* **296**, 910–913 (2002).

21. Barabási, A.-L. & Albert, R. Emergence of scaling in random networks. *Science* **286**, 509–512 (1999).

22. Cancho, R. F. I. & Solé, R. V. The small world of human language. *Proc. R. Soc. Lond., B, Biol. Sci.* **268**, 2261–2265 (2001).

23. Newman, M. E. The structure of scientific collaboration networks. *Proc. Natl. Acad. Sci. U.S.A.* **98**, 404–409 (2001).

24. Goh, K.-I., Kahng, B. & Kim, D. Universal behavior of load distribution in scale-free networks. *Phys. Rev. Lett.* **87**, 278701 (2001).

25. Liu, Y.-Y., Slotine, J.-J. & Barabási, A.-L. Controllability of complex networks. *Nature* **473**, 167 (2011).

26. Girvan, M. & Newman, M. E. Community structure in social and biological networks. *Proc. Natl. Acad. Sci. U.S.A.* **99**, 7821–7826 (2002).

27. Motter, A. E., De Moura, A. P., Lai, Y.-C. & Dasgupta, P. Topology of the conceptual network of language. *Phys. Rev. E* **65**, 065102 (2002).

28. Eriksen, K. A., Simonsen, I., Maslov, S. & Sneppen, K. Modularity and extreme edges of the internet. *Phys. Rev. Lett.* **90**, 148701 (2003).

29. Ravasz, E. & Barabási, A.-L. Hierarchical organization in complex networks. *Phys. Rev. E* **67**, 026112 (2003).

30. Deacon, T. W. *The symbolic species: The co-evolution of language and the brain* (WW Norton & Company, 1998).

31. Dix, A. *Human-computer interaction* (Springer, 2009).

32. Hayes, A. F. *Statistical methods for communication science* (Routledge, 2009).

33. Schall, R. Estimation in generalized linear models with random effects. *Biometrika* **78**, 719–727 (1991).

34. Strogatz, S. H. Exploring complex networks. *Nature* **410**, 268 (2001).

35. Albert, R. & Barabási, A.-L. Statistical mechanics of complex networks. *Rev. Mod. Phys.* **74**, 47 (2002).

36. Cleeremans, A. & McClelland, J. L. Learning the structure of event sequences. *J. Exp. Psychol. Gen.* **120**, 235 (1991).

37. Fiser, J. & Aslin, R. N. Statistical learning of higher-order temporal structure from visual shape sequences. *J. Exp. Psychol.* **28**, 458 (2002).

38. Newport, E. L. & Aslin, R. N. Learning at a distance I. Statistical learning of non-adjacent dependencies. *Cogn. Psychol.* **48**, 127–162 (2004).

39. Rosvall, M. & Bergstrom, C. T. An information-theoretic framework for resolving community structure in complex networks. *Proc. Natl. Acad. Sci. U.S.A.* **104**, 7327–7331 (2007).

40. Newman, M. E. The structure and function of complex networks. *SIAM Rev.* **45**, 167–256 (2003).

41. Sinatra, R., Gómez-Gardenes, J., Lambiotte, R., Nicosia, V. & Latora, V. Maximal-entropy random walks in complex networks with limited information. *Phys. Rev. E* **83**, 030103 (2011).

42. Demetrius, L. & Manke, T. Robustness and network evolutionan entropic principle. *Physica A* **346**, 682–696 (2005).

43. Burda, Z., Duda, J., Luck, J.-M. & Waclaw, B. Localization of the maximal entropy random walk. *Phys. Rev. Lett.* **102**, 160602 (2009).

44. Coghi, F., Morand, J. & Touchette, H. Large deviations of random walks on random graphs. *Phys. Rev. E* **99**, 022137 (2019).

45. Wickelgren, W. A. Speed-accuracy tradeoff and information processing dynamics. *Acta Psychol.* **41**, 67–85 (1977).

46. Ortega, P. A. & Braun, D. A. Thermodynamics as a theory of decision-making with information-processing costs. *Proc. R. Soc. A* **469**, 20120683 (2013).

47. Rieke, F. & Warland, D. *Spikes: exploring the neural code* (MIT press, 1999).

48. Delgado-Bonal, A. & Martín-Torres, J. Human vision is determined based on information theory. *Sci. Rep.* **6**, 36038 (2016).

49. Hyman, R. Stimulus information as a determinant of reaction time. *J. Exp. Psychol.* **45**, 188 (1953).

50. Karuza, E. A., Thompson-Schill, S. L. & Bassett, D. S. Local patterns to global architectures: Influences of network topology on human learning. *Trends Cogn. Sci.* **20**, 629–640 (2016).

51. Karuza, E. A., Kahn, A. E. & Bassett, D. S. Human sensitivity to community structure is robust to topological variation. *Complexity* **2019** (2019).

52. Howard, M. W. & Kahana, M. J. A distributed representation of temporal context. *J. Math. Psychol.* **46**, 269–299 (2002).

53. Dayan, P. Improving generalization for temporal difference learning: The successor representation. *Neural Comput.* **5**, 613–624 (1993).

54. Nobre, A. C. & van Ede, F. Anticipated moments: Temporal structure in attention. *Nat. Rev. Neurosci.* **19**, 34 (2018).

55. Sternberg, S. Memory-scanning: Mental processes revealed by reaction-time experiments. *Am. Sci.* **57**, 421–457 (1969).

56. Johnson-Laird, P. N. Mental models in cognitive science. *Cogn. Sci.* **4**, 71–115 (1980).

57. Winograd, E. & Lynn, D. S. Role of contextual imagery in associative recall. *Mem. Cogn.* **7**, 29–34 (1979).

58. Bousfield, W. A. The occurrence of clustering in the recall of randomly arranged associates. *J. Gen. Psychol.* **49**, 229–240 (1953).

59. Friederici, A. D. Neurophysiological markers of early language acquisition: From syllables to sentences. *Trends Cogn. Sci.* **9**, 481–488 (2005).

60. Gopnik, A. & Wellman, H. M. Reconstructing constructivism: Causal models, bayesian learning mechanisms, and the theory theory. *Psychol. Bull.* **138**, 1085 (2012).

61. Tompson, S. H., Kahn, A. E., Falk, E. B., Vettel, J. M. & Bassett, D. S. Individual differences in learning social and non-social network structures. *J. Exp. Psychol. Learn. Mem.Cogn.* (2018).

62. Reynolds, J. R., Zacks, J. M. & Braver, T. S. A computational model of event segmentation from perceptual prediction. *Cogn. Sci.* **31**, 613–643 (2007).

63. Piantadosi, S. T., Tenenbaum, J. B. & Goodman, N. D. Bootstrapping in a language of thought: A formal model of numerical concept learning. *Cognition* **123**, 199–217 (2012).

64. Tenenbaum, J. B., Griffiths, T. L. & Kemp, C. Theory-based bayesian models of inductive learning and reasoning. *Trends Cogn. Sci.* **10**, 309–318 (2006).

65. Meyniel, F. & Dehaene, S. Brain networks for confidence weighting and hierarchical inference during probabilistic learning. *Proc. Natl. Acad. Sci. U.S.A.* 201615773 (2017).

66. Jazayeri, M. & Shadlen, M. N. Temporal context calibrates interval timing. *Nat. Neurosci.* **13**, 1020 (2010).

67. Estrada, E. & Hatano, N. Communicability in complex networks. *Phys. Rev. E* **77**, 036111 (2008).

68. McCarthy, G. & Donchin, E. A metric for thought: A comparison of p300 latency and reaction time. *Science* **211**, 77–80 (1981).

69. Baayen, R. H., Davidson, D. J. & Bates, D. M. Mixed-effects modeling with crossed random effects for subjects and items. *J. Mem. Lang.* **59**, 390–412 (2008).

70. Bates, D., Mächler, M., Bolker, B., Walker, S. *et al.* Fitting linear mixed-effects models using lme4. *J. Stat. Softw.* **67** (2015).

71. Baddeley, A. D. & Hitch, G. The recency effect: Implicit learning with explicit retrieval? *Mem. Cogn.* **21**, 146–155 (1993).

72. Erdös, P. & Rényi, A. On random graphs I. *Publ. Math. Debrecen* **6**, 290–297 (1959).

73. Pastor-Satorras, R. & Vespignani, A. Epidemic spreading in scale-free networks. *Phys. Rev. Lett.* **86**, 3200 (2001).

74. Albert, R., Jeong, H. & Barabási, A.-L. Error and attack tolerance of complex networks. *Nature* **406**, 378 (2000).

75. Molloy, M. & Reed, B. A critical point for random graphs with a given degree sequence. *Random Struct. Algor.* **6**, 161–180 (1995).

76. Catanzaro, M. & Pastor-Satorras, R. Analytic solution of a static scale-free network model. *Eur. Phys. J. B* **44**, 241–248 (2005).

77. Lee, J.-S., Goh, K.-I., Kahng, B. & Kim, D. Intrinsic degree-correlations in the static model of scale-free networks. *Eur. Phys. J. B* **49**, 231–238 (2006).

78. Barabási, A.-L. *et al.* Evolution of the social network of scientific collaborations. *Physica A* **311**, 590–614 (2002).

79. Karrer, B., Newman, M. E. & Zdeborová, L. Percolation on sparse networks. *Phys. Rev. Lett.* **113**, 208702 (2014).

80. Decelle, A., Krzakala, F., Moore, C. & Zdeborová, L. Asymptotic analysis of the stochastic block model for modular networks and its algorithmic applications. *Phys. Rev. E* **84**, 066106 (2011).

81. Ravasz, E., Somera, A. L., Mongru, D. A., Oltvai, Z. N. & Barabási, A.-L. Hierarchical organization of modularity in metabolic networks. *Science* **297**, 1551–1555 (2002).

82. Arenas, A., Diaz-Guilera, A. & Pérez-Vicente, C. J. Synchronization reveals topological scales in complex networks. *Phys. Rev. Lett.* **96**, 114102 (2006).

83. Arenas, A., Fernandez, A. & Gomez, S. Analysis of the structure of complex networks at different resolution levels. *New J. Phys.* **10**, 053039 (2008).

84. Zamora-López, G., Chen, Y., Deco, G., Kringelbach, M. L. & Zhou, C. Functional complexity emerging from anatomical constraints in the brain: the significance of network modularity and rich-clubs. *Sci. Rep.* **6**, 38424 (2016).

85. Shakespeare, W. *The complete works of William Shakespeare* (Wordsworth Editions, 2007).

86. Pope, A., Buckley, T. A. *et al. The Iliad of Homer* (WW Gibbings, 1891).

87. Jowett, B. *The republic of Plato* (Clarendon press, 1888).

88. Austen, J. *Pride and prejudice* (Broadview Press, 2001).

89. Blake, W. *Songs of Innocence and of Experience*, vol. 5 (Princeton University Press, 1998).

90. Cervantes, M. *Don Quixote* (LBA, 2018).

91. Whitman, W. *Leaves of grass* (Oregan Publishing, 2017).

92. Kunegis, J. Konect: The Koblenz network collection. In *Proceedings of the 22nd International Conference on World Wide Web*, 1343–1350 (ACM, 2013).

93. Kiss, G. R., Armstrong, C., Milroy, R. & Piper, J. An associative thesaurus of English and its computer analysis. In *The computer and literary studies*, 153–165 (Edinburgh University Press, 1973).

94. Batagelj, V. & Mrvar, A. Pajek datasets. $<$*vlado.fmf.uni-lj.si/pub/networks/data/* $>$ (2006).

95. Roget, P. M. *Roget's Thesaurus of English Words and Phrases* (TY Crowell Company, 1911).

96. Howe, D. The free on-line dictionary of computing. $<$*foldoc.org* $>$ (1993).

97. Reitz, J. M. *Online dictionary for library and information science* (Libraries Unlimited, 2010).

98. Palla, G., Farkas, I. J., Pollner, P., Derényi, I. & Vicsek, T. Directed network modules. *New J. Phys.* **9**, 186 (2007).

99. Gleich, D., Zhukov, L. & Berkhin, P. Fast parallel pagerank: A linear system approach. In *Yahoo! Research Technical Report YRL-2004-038*, vol. 13, 22 (2004).

100. Rossi, R. A. & Ahmed, N. K. The network data repository with interactive graph analytics and visualization. In *Proceedings of the Twenty-Ninth AAAI Conference on Artificial Intelligence* (2015).

101. De Nooy, W., Mrvar, A. & Batagelj, V. *Exploratory social network analysis with Pajek*, vol. 27 (Cambridge University Press, 2011).

102. Boldi, P., Codenotti, B., Santini, M. & Vigna, S. UbiCrawler: A scalable fully distributed web crawler. *Software Pract. Exper.* **34**, 711–726 (2004).

103. Adamic, L. A. & Glance, N. The political blogosphere and the 2004 us election: divided they blog. In *Proceedings of the 3rd international workshop on Link discovery*, 36–43 (ACM, 2005).

104. Castillo, C., Chellapilla, K. & Denoyer, L. Web spam challenge 2008. In *Proceedings of the 4th International Workshop on Adversarial Information Retrieval on the Web* (2008).

105. Leskovec, J., Kleinberg, J. & Faloutsos, C. Graph evolution: Densification and shrinking diameters. *ACM Trans. Knowl. Discov. Data* **1**, 2 (2007).

106. Šubelj, L. & Bajec, M. Model of complex networks based on citation dynamics. In *Proceedings of the 22nd international conference on World Wide Web*, 527–530 (ACM, 2013).

107. Ley, M. The dblp computer science bibliography: Evolution, research issues, perspectives. In *International symposium on string processing and information retrieval*, 1–10 (Springer, 2002).

108. Viswanath, B., Mislove, A., Cha, M. & Gummadi, K. P. On the evolution of user interaction in facebook. In *Proceedings of the 2nd ACM workshop on Online social networks*, 37–42 (ACM, 2009).

109. Moody, J. Peer influence groups: Identifying dense clusters in large networks. *Soc. Netw.* **23**, 261–283 (2001).

110. Coleman, J. S. *et al. Introduction to mathematical sociology.* (London Free Press Glencoe, 1964).

111. Gleiser, P. M. & Danon, L. Community structure in jazz. *Adv. Complex Syst.* **6**, 565–573 (2003).

112. Zachary, W. W. An information flow model for conflict and fission in small groups. *J. Anthropol. Res.* **33**, 452–473 (1977).

113. Jackson, M. Thriller (1984).

114. The Beatles. A hard day's night (1964).

115. Queen. Bohemian rhapsody (1975).

116. Toto. Africa (1982).

117. Mozart, W. A. Piano sonata no. 11 (1784).

118. Beethoven, L. v. Piano sonata no. 23 (1807).

119. Chopin, F. Nocturnes, op. 9, no. 2 (1832).

120. Bach, J. S. The well-tempered clavier, book I, no. 13 (1722).

121. Brahms, J. Ballades, op. 10, no. 1 (1854).